Physics – Uspekhi **64** (12) 1286 – 1310 (2021)

PHYSICS OF OUR DAYS

PACS numbers: **12.60.–i**, 12.60.Cn, 13.20.Cz

50th ANNIVERSARY OF THE INSTITUTE FOR NUCLEAR RESEARCH, RAS

Search for light dark matter in the NA64 experiment

S N Gninenko, N V Krasnikov, V A Matveev

DOI: https://doi.org/10.3367/UFNe.2021.09.039066

Contents

Abstract. **We review the most important models of light dark matter and discuss the NA64 experiment aimed at searching for hypothetical particles, including dark matter, in the mass range $\leqslant O(1)$ GeV with the use of electron and muon beams at the Super Proton Synchrotron (SPS) accelerator at CERN. We consider the methods and results of searches in the NA64 and other accelerator experiments and also discuss their further prospects.**

Keywords: physics beyond the Standard Model, light dark matter

1. Introduction

At present, the leading experiments in high-energy and elementary particle physics can be conventionally divided into three groups. The first comprises experiments aimed at searches for new large-mass particles and manifestations of new physics beyond the Standard Model (SM) at small distances, i.e., in processes with large transferred momenta. A typical, and perhaps so far the sole, example is provided by the CMS (Compact Muon Solenoid) and ATLAS (A Toroidal LHC ApparatuS) experiments at the LHC (Large Hadron Collider) at CERN. Experiments of the second type amount to more accurate measurements of previously measured quantities. One of the most representative examples is given by experiments on measuring the $K \to \pi\nu\nu$ decay rate and anomalous magnetic moments of the muon and the electron in order to compare experimental data with theoretical predictions. The availability of reliable theoretical calculations is critical for experiments of this type. The third group includes experiments aimed at searches for rare processes, for example, $\mu \to e\gamma$ and eee decays, and new relatively light hypothetical particles with mass $m \leqslant O(1)$ GeV, such as axions, majorons, and dark photons. Evidently, if such particles exist, their coupling constants to ordinary matter particles (quarks, leptons, and photons) must be very small; otherwise, such particles would have already been discovered. Therefore, searching for them requires experiments at the maximum possible beam intensities, which places them into the domain of the so-called high-intensity frontier. Interest in experiments of this kind has especially increased recently in connection with the problem of dark matter.

S N Gninenko [1,a], **N V Krasnikov** [1,2], **V A Matveev** [1,2]
[1] Institute for Nuclear Research, Russian Academy of Sciences, prosp. 60-letiya Oktyabrya 7a, 117312 Moscow, Russian Federation
[2] Joint Institute for Nuclear Research, ul. Joliot-Curie 6, 141980 Dubna, Moscow region, Russian Federation
E-mail: [a] sergei.gninenko@cern.ch

Received 26 May 2021, revised 16 September 2021
Uspekhi Fizicheskikh Nauk **191** (12) 1361 – 1386 (2021)
Translated by S Alekseev

Currently, as is known, the most convincing evidence in favor of the existence of physics outside the SM, in addition to the detection of neutrino oscillations, is astronomical observations indicating the presence of dark matter (DM) in the Universe [1, 2].[1] The nature of DM is one of the most interesting issues in modern physics. If DM is a thermal relic, which at an early stage of the expansion of the Universe was in thermodynamic equilibrium with ordinary matter and then decoupled from it as the Universe cooled, then the interaction of DM with our matter must match the weak interaction by an order of magnitude. This is a strong motivation for developing models with new nongravitational interactions between DM and our matter.

Currently, among the many explanations for the origin of DM [1, 2], models of light dark matter (LDM) [4–12] with a particle mass less than $O(1)$ GeV have become very popular. Initially, such models were not discussed, because their naive versions led to predictions of the DM density in the Universe and constraints on the LDM mass that contradicted observations [13] (also see [14]). But with the appearance of a class of models containing additional interactions between ordinary and DM particles [4–12], these constraints were overcome. As mentioned above, as the Universe expands, DM particles leave thermodynamic equilibrium, i.e., decouple, at the moment the temperature and the corresponding annihilation cross section DM particles $\to$ SM particles and (or) the DM density become too small to maintain thermodynamic equilibrium.

Experimental data [1, 2] indicate that a scenario is realized in which the DM particles are nonrelativistic at the moment of decoupling; the mass of DM particles is much higher than the decoupling temperature. The annihilation cross section of DM particles into particles of our matter determines the residual DM density. Too large an annihilation cross section leads to a low DM density, and, conversely, too small an annihilation cross section leads to a high DM density. The observed value of the DM fraction $\rho_{\mathrm{D}}/\rho_{\mathrm{c}} \approx 0.25$ [15] allows finding the annihilation cross section of DM particles into particles of ordinary matter and assessing the prospects for the discovery of DM particles in accelerators. For example, in the model with a dark photon, the annihilation cross section $\sigma(\chi\bar{\chi} \to \mathrm{e}^+\mathrm{e}^-)$ is predicted to be $O(1)$ pbarn, and hence the cross section of the reverse process is of the same order of magnitude, which implies the possibility, in principle, of detecting LDM in accelerators.

Of course, the statement about the possibility of detecting LDM with accelerators depends on the specific model (see Sections 3–5). We note that the predicted annihilation cross section of DM particles into SM particles at the moment they leave thermodynamic equilibrium is weakly dependent on the mass of the DM particles [1, 2]. Astrophysical constraints, together with those derived from nucleosynthesis, are much more stringent than the corresponding accelerator constraints at LDM particle masses less than $O(1)$ MeV (see Section 4), while at LDM particle masses greater than $O(1)$ MeV, astrophysical constraints are typically weaker than the accelerator ones.

Models with LDM can be classified according to the spin of the particles and the mediator that carries the interaction between the hidden-sector and visible-matter particles. Models with scalar mediators are severely constrained by data [16, 17] on rare K- and B-meson decays, but are not excluded [18]. The model with a light vector mediator, a dark photon [5–20], is currently very popular. One of the reasons for the increased attention to this particular model is its simplicity and renormalizability. The interaction between SM and LDM particles arises due to a nonzero mixing between the photon and the dark photon A$'$, which is the vector mediator that carries interaction in the dark sector. However, other models are also possible, for example, those with $L_\mu - L_\tau$, $B-L$, and $B-3L_{\mathrm{e}}$ couplings of the vector mediator to LDM particles [21–27]. We emphasize that A$'$ should not be identified with LDM, although the dark photon can also be a candidate for a DM particle at a very small mixing and small masses.[2]

We note that there are currently no theoretical or experimental indications in favor of small ($O(1)$ GeV) masses of DM particles, nor indeed in favor of any other masses. At the same time, the experimental constraints on LDM models by no means exclude them. We note that one more indication in favor of the existence of physics beyond the SM is associated with the so-called muon $g_\mu - 2$ anomaly — the presence of a discrepancy at the 4.2σ level between the measured [28] and SM-predicted [29–32] values of the anomalous magnetic moment of the muon. Among the possible explanations for the $g_\mu - 2$ anomaly [33–36], we note models predicting the existence of a new light vector boson coupled mainly to leptons of the second and third generations via the $L_\mu - L_\tau$ lepton current [21–23].

As mentioned above, the possible existence of LDM is very attractive for experimental searches. Calculations show that the range of masses and coupling constants explaining the relict density of LDM lie in a range that is difficult, but not impossible to access in modern accelerator experiments. This has greatly stimulated additional efforts to develop new methods and improve the sensitivity of experiments to search for LDM. One such approach, developed in the NA64 experiment, is based on the search for 'energy nonconservation' (missing energy) in reactions involving the scattering of charged leptons by nuclei. Much attention is also attracted to such processes because their observation certainly goes beyond the SM framework and requires its significant extension. The possible discovery of DM in the Universe certainly increases the interest in such searches.

The purpose of this review is to consider the NA64 experiment for the search for hypothetical particles, including DM, in a mass range less than 1 GeV using electron and muon beams at the SPS (Super Proton Synchrotron) accelerator at CERN [37–43]. The experiment has the best sensitivity to date in the vector mediator mass range $O(1)$ MeV $\leqslant m_{\mathrm{A}'} \leqslant O(500)$ MeV. In addition, we discuss a number of other existing and planned experiments that are the most prominent competitors of NA64 in searches for LDM particles and mediators of their interactions. We also consider the phenomenology associated with a dark photon and LDM particles.

This review is organized as follows. In Section 2, we consider phenomenological aspects of LDM models, in particular, the dark photon model. In that same section, we also give an overview of the principal models involving new light particles capable of explaining the muon $(g_\mu - 2)$ anomaly. We present the basic formulas required to calculate

[1] We note attempts to explain astronomical observations by modifying the general relativity theory at long distances [3].

[2] We do not consider this possibility in this review, because it would make the NA64 experiment noncompetitive with other experiments [5–12].

the LDM density in the Universe. We also consider the main reactions used in accelerators to search for LDM and light mediators of its interactions with the SM. Section 3 is devoted to the NA64 experiment for the search for LDM particles and other hypothetical particles of the hidden sector. We describe the method for such a search in the NA64 experiment with electron and muon beams. The main results of the experiment are presented, and the prospects for further searches for LDM and other hypothetical particles are discussed. In Section 4, we discuss other accelerator and nonaccelerator constraints on light boson models, including LDM models. In Section 5, we briefly describe future experiments to search for LDM and the dark photon. In Section 6, we give our concluding remarks.

2. Phenomenological aspects of light dark matter models

2.1 Dark photon model

The most popular and best developed LDM model is the one with a vector carrier of the interaction between the observed matter and LDM, the dark photon model [6, 20]. In this model, a dark photon (a new massive vector boson A$'$) interacts with the SM $\mathrm{SU_c}(3)\otimes\mathrm{SU_L}(2)\otimes\mathrm{U}(1)$ gauge fields via nonzero mixing of the $\mathrm{U}'(1)$ A'_μ gauge field with the SM gauge field $\mathrm{U}(1)$ B_μ. The A$'$ field also couples to LDM fields. In renormalizable models with an extra abelian gauge group $\mathrm{U}'(1)$, the LDM particles have spin 0 or 1/2. [3] The Lagrangian of the model with a dark photon has the form

$$L = L_{\mathrm{SM}} + L_{\mathrm{SM,\,dark}} + L_{\mathrm{dark}}\,, \tag{1}$$

where L_{SM} is the SM Lagrangian,

$$L_{\mathrm{SM,\,dark}} = -\frac{\epsilon}{2\cos\theta_{\mathrm{W}}}B^{\mu\nu}F'_{\mu\nu}\,, \tag{2}$$

$B^{\mu\nu} = \partial^\mu B^\nu - \partial^\nu B^\mu$, $F'_{\mu\nu} = \partial_\mu A'_\nu - \partial_\nu A'_\mu$, ϵ is the mixing parameter, L_{dark} is the LDM Lagrangian, and θ_{W} is the Weinberg angle.

Currently, scalar, Dirac, Majorana, and pseudo-Dirac LDM models are mostly considered. [4] For the scalar model, the Lagrangian has the form

$$\begin{aligned} L_{\mathrm{dark}} = &-\frac{1}{4}F'_{\mu\nu}F'^{\mu\nu} + (\partial_\mu\chi - \mathrm{i}e_{\mathrm{D}}A'_\mu\chi)(\partial^\mu\chi - \mathrm{i}e_{\mathrm{D}}A'^\mu\chi)^* \\ &- m_\chi^2\chi^*\chi - \lambda_\chi(\chi^*\chi)^2 + \frac{m_{\mathrm{A}'}^2}{2}A'_\mu A'^\mu\,, \end{aligned} \tag{3}$$

where χ is an LDM charged scalar field, and e_{D} and λ_χ are coupling constants. Here, the gauge symmetry

$$A'_\mu \to A'_\mu + \partial_\mu\alpha\,, \tag{4}$$

$$\chi \to \exp(\mathrm{i}e_{\mathrm{D}}\alpha)\chi\,, \tag{5}$$

where α is an arbitrary function of coordinates, is broken explicitly by the nonvanishing mass term $(m_{\mathrm{A}'}^2/2)A'_\mu A'^\mu$ in Lagrangian (3). For the dark photon A'_μ to have mass, we can use the Higgs mechanism with the Lagrangian

$$L_\phi = (\partial_\mu\phi - \mathrm{i}e_{\mathrm{D}}A'_\mu\phi)(\partial^\mu\phi - \mathrm{i}e_{\mathrm{D}}A'^\mu\phi)^* - \lambda(\phi^*\phi - c^2)^2\,, \tag{6}$$

where c is an arbitrary constant leading to a nonzero mass [5] of A$'$ in the case of a nonzero vacuum expectation value, $\langle\phi\rangle \neq 0$. Due to nonzero mixing (2), the low-energy coupling of the dark photon A$'$ to SM fermions is described by the effective Lagrangian

$$L_{\mathrm{A}',\,\mathrm{SM}} = \epsilon e A'_\mu J^\mu_{\mathrm{EM}}\,, \tag{7}$$

where J^μ_{EM} is the SM electromagnetic current.

For Dirac LDM χ, the Lagrangian has the form

$$\begin{aligned} L_{\mathrm{dark}} = &-\frac{1}{4}F'_{\mu\nu}F'^{\mu\nu} + \mathrm{i}\bar\chi\gamma^\mu\partial_\mu\chi - m_\chi\bar\chi\chi \\ &+ e_{\mathrm{D}}\bar\chi\gamma^\mu\chi A'_\mu + \frac{m_{\mathrm{A}'}^2}{2}A'_\mu A'^\mu\,. \end{aligned} \tag{8}$$

For Majorana LDM described by χ_{M} (with $\chi_{\mathrm{M}} = \chi_{\mathrm{L}} + \chi_{\mathrm{L}}^{\mathrm{c}}$, $\chi_{\mathrm{M}}^{\mathrm{c}} = \chi_{\mathrm{M}}$, $\chi_{\mathrm{M}}^{\mathrm{c}} = C\bar\chi_{\mathrm{M}}$), [6] the main difference from the Dirac LDM is given by the replacement [11] $e_{\mathrm{D}}\bar\chi\gamma^\mu\chi A'_\mu \to (e_{\mathrm{D}}/2)\bar\chi_{\mathrm{M}}\gamma^\mu\gamma_5\chi_{\mathrm{M}}A'_\mu$ in Lagrangian (8), where the γ^μ are Dirac's gamma matrices and γ_5 is Dirac's gamma-5 matrix. In the model with pseudo-Dirac fermions [11, 54], introducing a scalar field ϕ_{PD} with a nonvanishing vacuum expectation value $\langle\phi_{\mathrm{PD}}\rangle \neq 0$ spontaneously breaks the fermion number, which is implemented by replacing the mass term $-m_\chi\bar\chi\chi \to -m_\chi\bar\chi\chi - (h_{\mathrm{PD}}\phi_{\mathrm{PD}}\bar\chi_{\mathrm{L}}^{\mathrm{c}}\chi_{\mathrm{L}} + h_{\mathrm{PD}}\phi_{\mathrm{PD}}\bar\chi_{\mathrm{R}}^{\mathrm{c}}\chi_{\mathrm{R}} + \mathrm{h.c.})$ in Lagrangian (8). The original Dirac fermion χ with a mass m_χ thus splits into two Majorana fermions: $\chi_{1,\,2\mathrm{M}} = \chi_{1,\,2} + \chi_{1,\,2}^{\mathrm{c}}$ with the masses [7] $m_{\chi_{1,\,2}} = m_\chi \mp 2h_{\mathrm{PD}}\langle\phi_{\mathrm{PD}}\rangle$. Here, $\chi_2 = (1/\sqrt{2})(\chi_{\mathrm{L}} + \chi_{\mathrm{R}}^{\mathrm{c}})$ and $\chi_1 = (-\mathrm{i}/\sqrt{2})(\chi_{\mathrm{L}} - \chi_{\mathrm{R}}^{\mathrm{c}})$. In the model with pseudo-Dirac fermions, A$'$ is coupled to pseudo-Dirac fermion fields by the replacement $e_{\mathrm{D}}\bar\chi\gamma^\mu\chi A'_\mu \to e_{\mathrm{D}}J^\mu_{\mathrm{PD}}A'_\mu$, $J^\mu_{\mathrm{PD}} = \mathrm{i}\bar\chi_2\gamma^\mu\chi_1 + \mathrm{h.c.}$ in Lagrangian (8). In the limit as $h_{\mathrm{PD}} \to 0$, we obtain a model with a Dirac fermion. In the early Universe, the pseudo-Dirac fermions χ_1 and χ_2 are produced in pairs and also annihilate in pairs. After leaving thermodynamic equilibrium, χ_2 decays into χ_1 and SM particles, for example, $\chi_2 \to \chi_1 + \mathrm{e}^+\mathrm{e}^-$. As a corollary, at later stages of expansion, the Universe contains only χ_1 LDM [54], which allows avoiding the constraint associated with the cosmic microwave background (CMB) radiation (see Section 4.4.1).

As we have already noted, the constraints on LDM models with a scalar portal are quite strong. This is because a renormalizable extension of the SM with additional scalar

[3] Models with spin-1 LDM particles are also possible [44–46]. For example, in the model in [47] with the dark sector gauge group $\mathrm{SU_X}(2)\times\mathrm{U_X}(1)$, after its breaking to the $\mathrm{U}'(1)$ gauge group, spin-1 bosons charged with respect to $\mathrm{SU_X}(2)$ can play the role of an LDM particle [47]. In addition, a light dark photon with a mass $m_{\mathrm{A}'} \ll m_{\mathrm{e}}$ is a candidate for an LDM particle [15]. In this review, we consider the simplest LDM models with spin 0 or 1/2.

[4] Millicharged particles can also be regarded as candidates for the role of LDM particles [48, 49], but their discussion goes beyond the scope of this review. Prospects for the search for millicharged particles in the NA64 experiment were addressed in [50].

[5] In models with spontaneous $\mathrm{U}'(1)$ gauge symmetry breaking, the corresponding 'Higgs boson' $S = (1/\sqrt{2})(\phi + \phi^* - \langle\phi\rangle - \langle\phi\rangle^*)$ can play the role of LDM [51] at small Higgs boson masses $m_{\mathrm{S}} \ll m_{\mathrm{A}'}$. For Higgs boson masses greater than the dark photon mass, its effect on the LDM density is insignificant [52, 53]. For masses $m_{\mathrm{S}} \approx m_\chi$ close to the mass of LDM particles, the $\chi\chi \to \mathrm{SS}$, $\mathrm{SS} \to \chi\chi$ annihilation processes considerably affect the LDM density and must be taken into account. Possible signatures for accelerator searches for the Higgs boson S were discussed in [52, 53].

[6] Here, $\chi_{\mathrm{L,\,R}} = (1 \mp \gamma_5)\chi/2$, $\chi^{\mathrm{c}} = C\bar\chi$, and $C = \mathrm{i}\gamma^0\gamma^2$ is the charge conjugation operator.

[7] We can always choose $\langle\phi_{\mathrm{PD}}\rangle > 0$, thereby ensuring that $m_{\chi_2} > m_{\chi_1}$.

mediators is possible only for models with additional scalar isodoublets and isosinglets, in particular, for a model with a scalar isosinglet and a scalar isodoublet coupled only to SM leptons [18], or for a model with several scalar isodoublets [24]. The simplest $SU_c(3) \otimes SU_L(2) \otimes U(1)$ SM extension by a scalar singlet mediator ϕ that mixes with the Higgs boson h allows explaining the observed LDM density, but contradicts the experimental constraint from rare K- and B-meson decays [17]. In models with several scalar isodoublets and an isosinglet [18, 24], after the electroweak $SU_L(2) \otimes U(1)$ symmetry breaking, a light scalar S appears in the spectrum, and its coupling to electrons can be represented as

$$L = (h_S \bar{e} e + \mathrm{i}\, h_P \bar{e} \gamma_5 e) S\,. \tag{9}$$

At the phenomenological level, we can thus obtain the experimental constraint on the coupling constants h_S and h_P (see Section 3).

In the model with a dark photon, estimating the coupling of LDM to ordinary SM matter requires knowing ϵ and $\alpha_D = e_D^2/(4\pi)$. Currently, we cannot predict their values from first principles, but we can obtain a constraint on α_D from above using the condition that the Landau pole of the effective coupling constant $\bar{\alpha}_D(\mu)$ be absent up to some scale Λ [55]. The one-Loop β function for the effective constant $\bar{\alpha}_D(\mu)$ has the form

$$\beta(\bar{\alpha}_D) = \frac{\bar{\alpha}_D^2}{2\pi} \left(\frac{4}{3} Q_F^2 n_F + Q_S^2 \frac{n_S}{3} \right), \tag{10}$$

where $\beta(\bar{\alpha}_D) \equiv \mu\, \mathrm{d}\bar{\alpha}_D/\mathrm{d}\mu$, n_F (n_S) is the number of fermions (scalars) with $U'(1)$ charges $Q_F(Q_S)$. For the model with pseudo-Dirac fermions, an extra scalar field ϕ_{PD} with the charge $Q_{PD} = 2$ must be introduced, and therefore the one-loop β function in that model is $\beta(\bar{\alpha}_D) = 4\bar{\alpha}_D^2/(3\pi)$.

For the model with a Majorana fermion, we also have to introduce an additional scalar field with the charge $Q_S = 2$ and an additional Majorana field to cancel the γ_5-anomalies, and therefore the β-function coincides with the β-function of the preceding model. In the model with scalar LDM, for the dark photon to acquire mass in a gauge-invariant way, an extra scalar field with the charge $Q_S = 1$ must be introduced, and hence the one-loop β-function has the form $\beta(\alpha_D) = \alpha_D^2/(3\pi)$. The condition $\Lambda \geqslant 1$ TeV implies that $\alpha_D \leqslant 0.2$ for pseudo-Dirac and Majorana fermions and $\alpha_D \leqslant 0.8$ for charged scalars. Here, α_D is the effective coupling constant on the scale $\mu = m_{A'}$, i.e., $\alpha_D = \bar{\alpha}_D(m_{A'})$.[8]

In our calculations, we use the value $m_{A'} = 10$ MeV as a 'reference' point, although the results depend weakly on the choice of a particular mass $m_{A'}$. Assuming that the dark photon model is applicable up to the Planck scale, i.e., $\Lambda = M_{PL} = 1.2 \times 10^{19}$ GeV, we obtain $\alpha_D \leqslant 0.05$ for pseudo-Dirac and Majorana fermions and $\alpha_D \leqslant 0.2$ for charged scalars. In the SM, the $SU_c(3)$, $SU_L(2)$, and $U(1)$ gauge coupling constants are $\sim (1/30-1/50)$ on the Planck scale. In our opinion, it is therefore natural to assume that the effective coupling constant $\bar{\alpha}_D(\mu = M_{PL})$ is in the range of the $SU_c(3)$, $SU_L(2)$, and $U(1)$ gauge constants, i.e., $\bar{\alpha}_D(\mu = M_{PL}) \sim (1/30-1/50)$. This implies that the values $\alpha_D \sim 0.01-0.02$ are the most natural ones.

In the pivotal work by Holdom [20], it was assumed that the appearance of the mixing parameter ϵ is associated with loop corrections coming from heavy particles that are charged electrically as well as with respect to the $U'(1)$ gauge group of the dark photon, and this ϵ parameter was evaluated at the level of $O(10^{-2}) \leqslant \epsilon \leqslant O(10^{-4})$. But other models also exist. In particular, a nonzero ϵ parameter can arise due to a nonrenormalizable coupling, for example, $-[\Phi/(2\Lambda)] F_{\mu\nu} F'^{\mu\nu}$. A nonzero vacuum expectation value $\langle \Phi \rangle \neq 0$ results in the nonzero mixing $\epsilon = \langle \Phi \rangle / \Lambda$. We note that the problem of the appearance of a nonzero mixing parameter was recently discussed in [56, 57]. In our opinion, there are currently no convincing predictions for the value of mixing, and we assume in what follows that ϵ is a free parameter of the theory, constrained only by experiment.

2.2 Decays and production of dark photons

Depending on the mass, A′ can decay into SM particles (visible modes), for example,

$$A' \to e^+e^-, \mu^+\mu^-, \pi^+\pi^-,$$

LDM particles (invisible modes),

$$A' \to \chi\bar{\chi},$$

and their mixture,[9]

$$A' \to \chi_1\chi_2,\ \chi_1 \to \chi_2 e^+e^-.$$

Invisible and visible widths of the dark photon decay into fermionic DM and electron–positron pairs can be expressed as[10]

$$\Gamma(A' \to \chi\bar{\chi}) = \frac{\alpha_D}{3} m_{A'} \left(1 + \frac{2m_\chi^2}{m_{A'}^2}\right) \sqrt{1 - \frac{4m_\chi^2}{m_{A'}^2}}, \tag{11}$$

$$\Gamma(A' \to e^+e^-) = \frac{\epsilon^2 \alpha}{3} m_{A'} \left(1 + \frac{2m_e^2}{m_{A'}^2}\right) \sqrt{1 - \frac{4m_e^2}{m_{A'}^2}}, \tag{12}$$

where $\alpha = e^2/(4\pi) = 1/137$.

There are several A′ production mechanisms [6]. In proton–nucleus collisions, dark photons A′ with a mass less than the mass of π^0, η, and η' mesons are mainly produced in the decays $\pi^0, \eta, \eta' \to \gamma A'$. The use of the visible decay $A' \to e^+e^-$ allows detecting the dark photon A′ as a peak in the e^+e^- invariant mass distribution. Direct A′ production in proton–nucleus interactions is also possible, in full analogy with photoproduction in such interactions.

Another effective way to produce A′ is to use the scattering of electrons on a nucleus, namely, the reaction (Fig. 1)

$$e^-(p) + Z(P_i) \to e^-(p') + Z(P_f) + A'(k)\,. \tag{13}$$

Here, $p = (E_0, \mathbf{p})$ is 4-momentum of the electron incident on the target, $P_i = (M, 0)$ is the 4-momentum of the nucleus Z in the initial state, $P_f = (P_f^0, \mathbf{P}_f)$ is the 4-momentum of the nucleus Z after the collision, $k = (k_0, \mathbf{k})$ is the 4-momentum of the A′ boson, and $p' = (p_0', \mathbf{p}')$ is the 4-momentum of the electron after collision. In the improved Weizsäcker–Wil-

[8] In [55], arguments are adduced in support of $\alpha_D \leqslant 0.1$.

[9] Which are not discussed in this review (see, e.g., [58]).

[10] For scalar DM particles χ, the invisible decay width of the dark photon is $\Gamma(A' \to \chi\chi^*) = (\alpha_D/12)\, m_{A'}(1 - 4m_\chi^2/m_{A'}^2)(1 - 4m_\chi^2/m_{A'}^2)^{1/2}$.

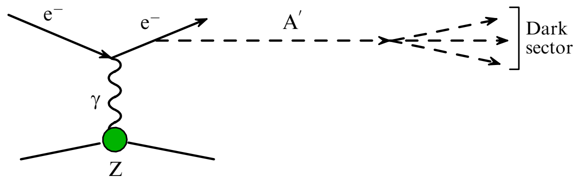

Figure 1. Diagram illustrating the production of a massive bremsstrahlung A′ boson in the reaction eZ → eZA′ with the subsequent invisible decay A′ → invisible.

liams (IWW) approximation, the differential and total cross sections for reaction (13) with $m_{A'} \gg m_e$ can be written as [59] [11]

$$\frac{d\sigma_{WW}^{A'}}{dx} = \left(4\alpha^3\epsilon^2\chi_{eff}\right)\left(1 - x + \frac{x^2}{3}\right) \times \left(m_{A'}^2\frac{1-x}{x} + m_e^2 x\right)^{-1}, \quad (14)$$

$$\sigma_{WW}^{A'} = \frac{4}{3}\,\frac{\epsilon^2\alpha^3}{m_{A'}^2}\log\delta_{A'}^{-1}, \quad (15)$$

$$\delta_{A'} = \max\left(\frac{m_e^2}{m_{A'}^2}, \frac{m_{A'}^2}{E_0^2}\right), \quad (16)$$

where $x = E_{A'}/E_0$, and χ_{eff} is the effective photon flux

$$\chi_{eff} = \int_{t_{min}}^{t_{max}} dt\,\frac{t - t_{min}}{t^2}\left(G_2^{el}(t) + G_2^{inel}(t)\right). \quad (17)$$

Here, $t_{min} = m_{A'}^4/(4E_0^2)$, $t_{max} = m_{A'}^2 + m_e^2$, and $G_2^{el}(t)$ and $G_2^{inel}(t)$ are the elastic and inelastic formfactors. For the NA64 energy $E \leqslant 100$ GeV, the elastic formfactor dominates. The elastic formfactor can be expressed as [59]

$$G_2^{el} = \left(\frac{a^2 t}{1 + a^2 t}\right)^2\left(\frac{1}{1 + t/d}\right)^2 Z^2, \quad (18)$$

where $a = 111Z^{-1/3}/m_e$, $d = 0.164$ GeV^2 $A^{-2/3}$, and A is the atomic number of the nucleus. We here consider quasielastic reactions (13), and therefore the inelastic nuclear formfactor is not taken into account. Numerically, $\chi_{eff} = Z^2$Log, and the function Log $\sim (5-10)$ depends weakly on the effects due to the finite size of the nucleus. Reaction (13) is the main source of A′ in the NA64 experiment.

2.3 Reactions used to search for light dark matter and dark photons in accelerators

We briefly describe the most interesting reactions used (or planned to be used) in searching for both visible and invisible decays of A′ with a mass $m_{A'} \leqslant O(1)$ GeV in accelerator experiments.

2.3.1 Visible decays of A′. Experiments on the search for visible decays $A' \to e^+e^-, \mu^+\mu^-, \pi^+\pi^-, \ldots$ are quite numerous [6]. They can be classified as searches using (a) $e^+e^- \to \gamma A'$ reactions on e^+e^- colliders, (b) $eZ \to eZA'$ in fixed-target experiments, and (c) decays of neutral mesons $\pi^0, \eta \to A'\gamma$, produced in proton–nucleus collisions pA, or the direct production of A′ in proton beam-dump experiments [6]. [12]

The A′ boson can be identified as a narrow resonance in the distribution of the invariant mass of an l^+l^- pair or, for example, from the decay vertex $A' \to l^+l^-$. Indeed, the decay length of the A′ boson is $L_d \sim E_{A'}/(\epsilon^2 m_{A'}^2)$ (where $E_{A'}$ is the energy of A'), and this means that the search for decay vertices remote from the interaction point allows obtaining constraints on the ϵ parameter. The disadvantage of this approach is that, in the region of the mixing parameters and masses where L_d is much larger than the characteristic size of the installation, the number of signal events in the experiment (or its sensitivity) is proportional to ϵ^4 (one ϵ^2 comes from the A′ production cross section, and the other from the A′ decay probability in the installation), and therefore the resultant constraints on ϵ are relatively weak [62]. For A′ with masses $m_{A'} \gtrsim 1$ GeV, the number of events in a reaction of type b is suppressed by the factor $1/m_{A'}^2$ in the A′ production cross section (see (15)) and, in addition, particles become extremely short-lived; therefore, searches for a resonance using type-a processes are preferable in that range.

2.3.2 Invisible decays of A′. LDM is produced in the reaction $eZ \to eZ(A' \to \chi\bar{\chi})$ or $e^+e^- \to \gamma(A' \to \chi\bar{\chi})$ and is identified by measuring the missing energy resulting from the undetectability of LDM particles. Of fundamental importance here is the air-tightness of the detector for suppressing background events. Studying the missing-mass distribution is also very effective in finding invisible A′ decays. For example, the BaBar collaboration [63] used the reaction $e^+e^- \to \gamma(A' \to \chi\chi)$. The momenta of e^+, e^-, and γ are measured with an accuracy of $O(10^{-2})$, which allows reconstructing the missing mass $m_{mis} = [(p_{e^+} + p_{e^-} - p_\gamma)^2]^{1/2}$ with good accuracy. The A′ boson is sought as a peak in the distribution of the invariant mass m_{mis}. However, there are experiments in which the measurement of the initial and final momenta is impossible. In the NA64 experiment [37], for example, the reaction $eZ \to eZA'$; $A' \to \chi\bar{\chi}$ (see Fig. 1) is used to search for invisible decays of A′, and only the energies of the initial and final electrons are measured. A typical signature of LDM particle detection is a large amount of energy missing in the detector. The high degree of air-tightness of the installation allows suppressing the background to the level of $O(10^{-12})$ and even lower, which is fundamentally important for the detection of A′. The number of signature events in the NA64 experiment is proportional to ϵ^2, the mixing parameter squared.

2.3.3 Proton and electron beam-dump experiments. In proton beam-dump experiments, LDM particles are produced in the decays $\pi^0, \eta, \eta' \to \gamma A'(A' \to \chi\bar{\chi})$ or in the direct production reaction $pZ \to pZA'(A' \to \chi\bar{\chi}) + \ldots$ and are detected by scattering reactions $\chi e \to \chi e$ and $\chi N \to \chi N$ on the electrons and nuclei of the target. [13]

These experiments 'probe' the LDM particles twice, and they are sensitive to the value of the fine coupling constant $\alpha_D = e_D^2/(4\pi)$ of the A′dark photon to LDM. The number of

[11] Exact calculations at the tree level for the reaction $e^-Z \to e^-ZA'$ have been done in [60, 61]. For some kinematic domains of the parameters $m_{A'}$ and $E_{A'}$, the yield of A′ bosons in the IWW approximation can differ significantly from that in exact tree-level calculations [60, 61].

[12] Decays of other mesons, $\eta' \to \gamma A'$, $K^* \to KA'$, make a smaller contribution.

[13] The reaction of elastic scattering $\chi Z \to \chi Z$ of LDM particles on a nucleus was used in the Coherent experiment for deriving constraints on LDM (see Section 4.2.4).

events registered in the far detector is proportional to $\sigma(\mathrm{pZ}\to\mathrm{pZ}(\mathrm{A}'\to\chi\bar{\chi})+\ldots)\sigma(\mathrm{e}\chi\to\mathrm{e}\chi)\sim\epsilon^2\epsilon^2\alpha_\mathrm{D}$, and therefore a large number of particles hitting the target are required, of the order of $1/\epsilon^4$. In electron beam-dump experiments, the A$'$ electroproduction reaction $\mathrm{eZ}\to\mathrm{eZA}'+\ldots$ is used, followed by the decay $\mathrm{A}'\to\chi\bar{\chi}$. In the far detector, elastic scattering reactions $\chi\mathrm{e}\to\chi\mathrm{e}$, $\chi\mathrm{N}\to\chi\mathrm{N}$ allow registering LDM particles.

2.4 Muon ($g_\mu - 2$) anomaly and the light vector boson

Accurate measurements of the anomalous magnetic moment of a positively charged muon $a_\mu=(g_\mu-2)/2$ at the Brookhaven National Laboratory (USA) [64] give a result approximately 3.6σ higher [65, 66] than the SM prediction:

$$a_\mu^{\mathrm{exp}}-a_\mu^{\mathrm{SM}}=(288\pm 80)\times 10^{-11}\,. \tag{19}$$

Recently, the Fermi National Accelerator Laboratory (Fermilab) collaboration announced a new result on measuring the anomalous magnetic moment of the muon [28]. The combined result of these two experiments is offset by 4.2σ from the theoretical prediction, namely, [28]

$$a_\mu^{\mathrm{exp}}-a_\mu^{\mathrm{SM}}=(251\pm 59)\times 10^{-11}\,. \tag{20}$$

These results might indicate the existence of new physics beyond the SM. A new light vector boson (dark photon) with a mass $m_{Z'}\leqslant O(1)$ GeV, weakly coupled to the muon, can explain the $(g_\mu-2)$ anomaly [33–36]. The vector coupling of the Z$'$ boson to the muon,

$$L_{Z'}=g'\bar{\mu}\gamma^\nu\mu Z'_\nu\,, \tag{21}$$

leads to an additional contribution to the anomalous magnetic moment of the muon [66],

$$\Delta a=\frac{\alpha'}{2\pi}\,F\left(\frac{m_{Z'}}{m_\mu}\right), \tag{22}$$

where

$$F(x)=\int_0^1 \mathrm{d}z\,\frac{2z(1-z)^2}{(1-z)^2+x^2z}\,, \tag{23}$$

and $\alpha'=(g')^2/(4\pi)\equiv\epsilon^2\alpha$.

Relations (22) and (23) allow finding the coupling constant α' responsible for the muon anomaly magnitude in (20). For $m_{Z'}\ll m_\mu$,

$$\alpha'=(1.6\pm 0.4)\times 10^{-8}\,. \tag{24}$$

In another limit case, $m_{Z'}\gg m_\mu$, the value of α' is

$$\alpha'=(2.4\pm 0.5)\times 10^{-8}\,\frac{m_{Z'}^2}{m_\mu^2}\,. \tag{25}$$

But postulating the coupling in (21) gives rise to more questions. One of them is: how do the other quarks and leptons couple to the Z$'$-boson? A renormalizable interaction of the Z$'$-boson with SM fermions ψ_k ($\psi_k=\mathrm{e},\nu_\mathrm{e},\mathrm{u},\mathrm{d},\ldots$) is given by

$$L_{Z'}=g'Z'_\mu J^\mu_{Z'} \tag{26}$$

$$J^\mu_{Z'}=\sum_k\left(q_{\mathrm{L}k}\bar{\psi}_{\mathrm{L}k}\gamma^\mu\psi_{\mathrm{L}k}+q_{\mathrm{R}k}\bar{\psi}_{\mathrm{R}k}\gamma^\mu\psi_{\mathrm{R}k}\right), \tag{27}$$

where $\psi_{\mathrm{L}k,\,\mathrm{R}k}=(1/2)(1\mp\gamma_5)\psi_k$, and $q_{\mathrm{L}k}$ and $q_{\mathrm{R}k}$ are the Z'-charges of the $\psi_{\mathrm{L}k}$- and $\psi_{\mathrm{R}k}$-fermions. Also, Z$'$ can be coupled to new hypothetical particles, for example, LDM fermions χ:

$$L_{Z'\chi}=g_\mathrm{D}Z'_\mu\bar{\chi}\gamma^\mu\chi\,. \tag{28}$$

There are several models predicting different forms of the $J^\mu_{Z'}$ current. In the model with a dark photon [20], the $\mathrm{Z}'(\equiv\mathrm{A}')$ boson interacts with the electromagnetic field A_μ as a result of nonzero mixing (2). Due to mixing (2), Z$'$ is coupled to the electromagnetic SM current

$$J^\mu_{\mathrm{EM}}=\frac{2}{3}\bar{u}\gamma^\mu u-\frac{1}{3}\bar{d}\gamma^\mu d-\bar{e}\gamma^\mu e+\ldots$$

with the coupling constant $g'=\epsilon e$. But experimental data exclude the model with the dark photon explaining the muon $(g_\mu-2)$ anomaly (see Sections 3 and 4).

In [33–35], as a proposal to explain the muon $(g_\mu-2)$ anomaly, a model was discussed where the Z$'$ boson is mainly coupled to only second- and third-generation leptons via the $L_\mu-L_\tau$ current:

$$L_{Z'}=g'\left[\bar{\mu}\gamma^\nu\mu+\bar{\nu}_{\mu\mathrm{L}}\gamma^\nu\nu_{\mu\mathrm{L}}-\bar{\tau}\gamma^\nu\tau-\bar{\nu}_{\tau\mathrm{L}}\gamma^\nu\nu_{\tau\mathrm{L}}\right]Z'_\nu\,. \tag{29}$$

The coupling in (29) is free of γ_5 anomalies, commutes with the SM gauge group, and does not contradict the experimental data for $m_{Z'}\leqslant 2m_\mu$ (see Section 4), mainly because (29) does not involve first-generation quarks and leptons. In [67], a model was proposed in which the Z$'$ boson is coupled to the right-handed currents of first- and second-generation SM fermions. The model explains the muon anomaly as a result of the existence of a light scalar in the spectrum.

2.5 Density of dark matter in the Universe

A discussion of the role of DM in the Universe is not the main topic of this review; for completeness, we present only the basic formulas that are needed to estimate the density of DM in the Universe. Experimental data [15] indicate the nonzero DM density $\Omega_\mathrm{D}\equiv\rho_\mathrm{D}/\rho_\mathrm{c}\approx 0.25$, while the contribution of ordinary matter is $\Omega_\mathrm{M}\equiv\rho_\mathrm{M}/\rho_\mathrm{c}\approx 0.04$. Here, ρ_D and ρ_M are the densities of DM and ordinary matter (made of SM particles), $\rho_\mathrm{c}=3H^2/(8\pi G_\mathrm{N})=1.05\times 10^{-5}\,h^2$ GeV cm^{-3} is the critical density of the Universe, and G_N is the gravitational constant. The parameter h is defined as $H\equiv 100\,h$ km s^{-1} Mpc^{-1} , where H is the Hubble constant. The experimental value is $h=0.674\pm0.005$ according to the 'Planck' collaboration data [15]. It thus follows from the experimental data that DM is currently dominant over ordinary matter. The generally accepted hypothesis is that, at an early stage of the expansion of the Universe, DM particles were in thermodynamic equilibrium with ordinary-matter particles, [14] but at a certain stage of the expansion they left thermodynamic equilibrium with SM matter. To calculate the density of DM, we have to solve the Boltzmann equation [1, 2, 68]

$$\frac{\mathrm{d}n_\mathrm{D}}{\mathrm{d}t}+3H(T)n_\mathrm{D}=-\langle\sigma v_{\mathrm{rel}}\rangle\left(n_\mathrm{D}^2-n_{\mathrm{D,eq}}^2\right), \tag{30}$$

[14] We emphasize that models exist in which DM was never in thermodynamic equilibrium with our matter at the early stages of cosmological expansion. In that case, the coupling constants of DM to our matter are typically very small, which makes the search for DM in accelerator and underground experiments an exceptionally challenging problem.

where

$$n_{\rm D}(T) = \int \frac{{\rm d}^3 p}{(2\pi)^3} f_{\rm D}(p, T)\,, \qquad (31)$$

$f_{\rm D}(p, T)$ is the density distribution of DM particles over momenta, $\langle\sigma v_{\rm rel}\rangle$ is the thermally averaged annihilation cross section of DM particles, $v_{\rm rel}$ is the relative speed of colliding particles, $n_{\rm D,\,eq}$ is the equilibrium density of LDM, and $H(T)$ is the Hubble parameter at a temperature T. In the nonrelativistic approximation, $\langle\sigma v_{\rm rel}\rangle = \sigma_0 (m_\chi/T)^{-n}$. The parameter value $n = 0$ corresponds to the s-wave annihilation of DM particles, and $n = 1$ corresponds to p-wave annihilation. An approximate solution of the Boltzmann equation for nonrelativistic DM particles leads to the following estimate [1, 69, 70] of the present-day density of DM:

$$\Omega_{\rm D} h^2 = k \frac{(n+1)\, x_{\rm f}^{n+1}}{g_{*,\,{\rm av}}^{1/2}} \left(\frac{8.77\times 10^{-11}\ {\rm GeV}^{-2}}{\sigma_0}\right). \qquad (32)$$

Here, $T_{\rm D}$ is the temperature at which DM particles leave thermodynamic equilibrium with SM particles, $x_{\rm f} = m_\chi/T_{\rm D}$, and g_* and g_{*s} are the numbers of relativistic degrees of freedom that determine the energy and entropy density, with $g_{*,\,{\rm av}}^{1/2} = g_{*s}/g_*^{1/2}$. If a DM antiparticle is not coincident with a DM particle, the parameter value is $k = 2$; otherwise, $k = 1$.

We have the following approximate formula for $x_{\rm f}$ [1, 69, 70]:

$$x_{\rm f} = c - \left(n + \frac{1}{2}\right)\ln c\,, \qquad (33)$$

$$c = \ln\left[0.038(n+1)\frac{g}{\sqrt{g_*}} M_{\rm Pl}\, m_\chi \sigma_0\right]. \qquad (34)$$

Here, g is the number of inner degrees of freedom of DM particles and $M_{\rm Pl} = 1.2\times 10^{19}$ GeV is the Planck mass. As a corollary of (32), given the s-wave annihilation cross section with $n = 0$ and $k = 2$, the cross section

$$\langle\sigma v_{\rm rel}\rangle = 7.3\times 10^{-10}\ {\rm GeV}^{-2} \frac{2}{g_{*,\,{\rm av}}^{1/2}} \frac{m_\chi}{T_{\rm D}} \qquad (35)$$

leads to the correct value of the present-day DM density. Calculations yield the estimate $1 \leqslant c_{\rm s} \equiv m_\chi/(10 T_{\rm D}) \leqslant 1.5$ for $1 \leqslant m_\chi \leqslant 100$ MeV. We note that the reaction $\chi\bar\chi \to {\rm e^-e^+}$ is the leading one at masses $1 \leqslant m_\chi \leqslant 100$ MeV. At higher masses, other annihilation reactions must be taken into account, such as $\chi\bar\chi \to \mu^-\mu^+,\ \pi^-\pi^+, + \ldots$. We consider the case $1 \leqslant m_\chi \leqslant 100$ MeV in what follows, i.e., take only the reaction $\chi\bar\chi \to {\rm e^-e^+}$ into account. For a Dirac fermion χ in the model with a dark photon in the nonrelativistic approximation, the annihilation cross section into an electron–positron pair having an s-wave nature is given by [11, 16] [15]

$$\sigma(\chi\bar\chi \to {\rm e^-e^+})v_{\rm rel} = \frac{16\pi\epsilon^2 \alpha\alpha_{\rm D} m_\chi^2}{(m_{\rm A'}^2 - 4m_\chi^2)^2}\,. \qquad (36)$$

It follows from (35) and (36) that

$$\epsilon^2\alpha_{\rm D} = 2\times 10^{-8}\,{\rm GeV}^{-2} \frac{(m_{\rm A'}^2 - 4m_\chi^2)^2}{m_\chi^2} \frac{2c_{\rm s}}{g_{*,\,{\rm av}}^{1/2}}\,. \qquad (37)$$

Given the commonly used relation $m_{\rm A'} = 3m_\chi$, we arrive at an estimate [16]

$$\epsilon^2\alpha_{\rm D} \sim 0.4\times 10^{-12}\left(\frac{m_\chi}{\rm MeV}\right)^2. \qquad (38)$$

We note that, for pseudo-Dirac LDM, the predicted value of $\epsilon^2\alpha_{\rm D}$ is greater than the corresponding value for Dirac LDM [11]. For the p-wave section, typical of scalar DM, the formula $\langle\sigma v_{\rm rel}\rangle = \langle B v_{\rm rel}^2\rangle = 6B(T/m_\chi)$ holds in the nonrelativistic approximation. An analogue of formula (35) that leads to the correct DM density has the form

$$6B = 14.6\times 10^{-10}\ {\rm GeV}^{-2} \frac{2}{g_{*,\,{\rm av}}^{1/2}} \left(\frac{m_\chi}{T_{\rm D}}\right)^2. \qquad (39)$$

For p-wave annihilation, the corresponding estimates at $1 \leqslant m_\chi \leqslant 100$ MeV lead to $m_\chi/T_{\rm D} = 10 c_{\rm p}$, where $1 \leqslant c_{\rm p} \leqslant 2$. For charged scalar LDM, the annihilation cross section in the nonrelativistic approximation is given by [11, 16]

$$\sigma v_{\rm rel} = \frac{8\pi}{3} \frac{\epsilon^2\alpha\alpha_{\rm D} m_\chi^2 v_{\rm rel}^2}{(m_{\rm A'}^2 - 4m_\chi^2)^2}\,. \qquad (40)$$

As a corollary of formulas (39) and (40), we find

$$\epsilon^2\alpha_{\rm D} = 4.0\times 10^{-7}\ {\rm GeV}^{-2} \frac{(m_{\rm A'}^2 - 4m_\chi^2)^2}{m_\chi^2} \frac{2c_{\rm p}^2}{g_{*,\,{\rm av}}^{1/2}}\,. \qquad (41)$$

At $m_{\rm A'} = 3m_\chi$, the estimate

$$\epsilon^2\alpha_{\rm D} \sim 10^{-11}\left(\frac{m_\chi}{\rm MeV}\right)^2 \qquad (42)$$

then follows. For a Majorana fermion, estimate (42) has an additional factor $\approx 1/2$.

We note that formulas (37) and (41) give a prediction for $\alpha_{\rm D}$ times ϵ^2 depending on the specific values of m_χ and $m_{\rm A'}$. As follows from (37) and (41), for $m_{\rm A'} \gg m_\chi$, the quantity $y \equiv (m_\chi/m_{\rm A'})^4 \alpha_{\rm D}\epsilon^2$ depends only on the mass of LDM particles, and therefore y is often used in the literature when comparing theoretical predictions and experimental constraints. We also note that the annihilation cross section is proportional to $x_{\rm f}^{n+1} = (m_\chi/T_{\rm D})^{n+1}$ and the quantity $m_\chi/T_{\rm D}$ then weakly depends on the LDM mass m_χ. Hence, the annihilation cross section leading to the observed LDM density also weakly depends on the LDM mass.

2.5.1 LDM and the Z' boson coupled to the $L_\mu - L_\tau$ current [24–27]. It is interesting to note that the current LDM density can be explained by an extension of the $L_\mu - L_\tau$ model to the dark sector. As an example, we consider an extension of the model with an LDM scalar field χ charged with respect to the ${\rm U}(1)_{L_\mu - L_\tau}$ gauge group. [17] The coupling of χ LDM particles to the Z' boson is described by the Lagrangian

$$L_{\chi Z'} = (\partial^\mu\chi - {\rm i}e_{\rm D} Z'^\mu\chi)^*(\partial_\mu\chi - {\rm i}e_{\rm D} Z'_\mu\chi) - m_\chi^2\chi^*\chi - \lambda_\chi(\chi^*\chi)^2\,. \qquad (43)$$

[15] Here, we assume that $m_\chi \gg m_{\rm e}$.

[16] The average value is $g_{*,\,{\rm av}}^{1/2} \approx 3.3$ for $10 \leqslant m_\chi \leqslant 100$ MeV.

[17] The annihilation cross section for scalar charged LDM is suppressed as a result of p-wave annihilation, which allows bypassing the constraint obtained from CMB anisotropy data [71].

The $\chi\bar{\chi} \to \nu_\mu\bar{\nu}_\mu, \nu_\tau\bar{\nu}_\tau$ annihilation cross section in the non-relativistic approximation $s \approx 4m_\chi^2$ is given by [18]

$$\sigma v_{\rm rel} = \frac{8\pi}{3} \frac{\epsilon^2 \alpha\alpha_{\rm D} m_\chi^2 v_{\rm rel}^2}{(m_{Z'}^2 - 4m_\chi^2)^2} \,. \tag{44}$$

We use the standard assumption that DM in the early Universe was in thermodynamic equilibrium with ordinary matter. Using formulas (32)–(34) and (44), we then find

$$\epsilon^2 \alpha_{\rm D} = k(m_\chi) \times 10^{-6} \left(\frac{m_\chi}{\rm GeV}\right)^2 \left(\frac{m_{Z'}^2}{m_\chi^2} - 4\right)^2 . \tag{45}$$

Here, the coefficient $k(m_\chi)$ depends logarithmically on the mass m_χ of LDM particles, and $k(m_\chi) \sim O(1)$ for $1 \leqslant m_\chi \leqslant 100$ MeV.

As noted previously, the model of a Z' boson coupled to the $L_\mu - L_\tau$ current can explain the muon $(g_\mu - 2)$ anomaly. For example, for $m_{Z'} \ll m_\mu$, the value of $\epsilon^2 = \alpha'/\alpha$ is determined by formula (24). It then follows from (45) that $\alpha_{\rm D}$ can be expressed as

$$\alpha_{\rm D} \sim 0.4 k(m_\chi) \left(\frac{m_\chi}{\rm GeV}\right)^2 \left(\frac{m_{A'}^2}{m_\chi^2} - 4\right)^2 . \tag{46}$$

In other words, the model of the Z' boson coupled to the $L_\mu - L_\tau$ current and LDM particles allows explaining both the muon $(g_\mu - 2)$ anomaly and the present-day LDM density in the Universe. In our opinion (see also, e.g., [72]), all this seriously increases the motivation for the search for Z' in the new setup of the NA64 experiment with a muon beam (see Section 3.5).

3. NA64 experiment

In this section, we describe the operating principles of the NA64 experiment and its main results and also discuss further prospects for the NA64 search for LDM, including the muon beam experiment.

3.1 General remarks

If the hypothetical A' boson exists, then it could be produced in the reaction of elastic scattering of high-energy electrons by the nuclei of an active target, similarly to bremsstrahlung photons,

$$eZ \to eZA', \; A' \to \chi\bar{\chi} \,, \tag{47}$$

with the subsequent rapid decay $A' \to \chi\bar{\chi}$ into LDM particles if $\alpha_{\rm D} \gg \epsilon^2$. The target is an active beam dump, an Electromagnetic CALorimeter (ECAL), capable of completely absorbing the energy E_0 of incident electrons.

The A' boson production cross section and therefore the number of A' produced are proportional to g_V^2, the squared vector coupling constant of A' to the electron. In the model with a dark photon, $g_V = \epsilon e$, and the number of produced A' is proportional to the mixing parameter squared, ϵ^2. As long as ϵ^2 is small, the decay of A' is invisible, $A' \to$ invisible, because A' and the χ particles are weakly coupled to matter and are not registered in a detector consisting of an ECAL target and a subsequent Hadron CALorimeter (HCAL).[19] For reaction (47), part of the energy of the primary electron is therefore carried away from the detector by particles resulting from the decay $A' \to \chi\bar{\chi}$, and the signature of the signal event consists of (a) the presence of energy release $E_{\rm ECAL}$ from an electron scattered in ECAL, accompanied by (b) the absence of energy release in HCAL [62]. In NA64, the constraints were deduced using the sensitivity-optimized signal region $E_{\rm miss} = E_0 - E_{\rm ECAL} \gtrsim 50$ GeV with the zero-energy threshold in HCAL $E_{\rm HCAL} \lesssim 1$ GeV, which allowed effectively suppressing the background of SM processes to the level of $\lesssim 10^{-13} - 10^{-12}$ per incoming electron (see Section 3.2). We note that this signature can also be used in NA64 to seek and derive constraints on the visible decays $A' \to e^-e^+$ when a long-lived A' carries away part of the incident electron energy from the installation and decays outside it.

To effectively suppress the background in the search for invisible decays of A' based on the $E_{\rm miss}$ signature, we need, first, a high level of reliability in identifying the incoming particle type and measuring its momentum. For example, if an incoming pion or kaon present in the beam is mistaken for an electron, it can decay on the fly into a state with lower-energy electrons, which can then simulate a signal. Second, a high air-tightness of the detector is needed to suppress the background coming from energy leaks in processes accompanied by the production of neutral hadrons (n, K_L^0) in the target.

It is worth noting the fundamental advantage of the active beam-dump target method used in the NA64 experiment and how it differs from the method of classical beam-dump experiments. In beam-dump searches, it is assumed that an A' produced in the beam absorber creates a χ-particle flux due to the decay $A' \to \chi\bar{\chi}$, which is detected in the far detector after passing through protection due to $\chi e \to \chi e$, $\chi N \to \chi N$ scattering on electrons or nuclei of the target. The number of signal events in the far detector is then proportional to $\sigma(eZ \to eA' + \ldots)\sigma(\chi e \to \chi e) \sim \epsilon^2 \epsilon^2 \alpha_{\rm D}$ [62].

As discussed above, the invisible decays $A' \to \chi\bar{\chi}$ are detected in the NA64 experiment indirectly by measuring the missing energy. Moreover, the production of an A' and its detection occur in the absorber target, which is simultaneously a calorimeter. That is why the NA64 experiment is said to use the active beam-dump method. The number of signal events in the experiment is proportional to ϵ^2, rather than $\epsilon^4 \alpha_{\rm D}$, as in the above-mentioned beam-dump searches with a passive target. Therefore, due to an extra factor of the order of ϵ^2, a relatively low flux of incident electrons in NA64 still allows obtaining much better constraints on the mixing parameter than in classic beam-dump experiments. For example, if $\epsilon \simeq 10^{-5}$, then the advantage of the NA64 method in terms of the number of primary particles required for signal detection is about 10 orders of magnitude. Because the number of signal events in beam-dump searches is proportional to $\epsilon^2 \times \epsilon^2 \alpha_{\rm D}$, the constraint on ϵ^2 for a fixed $\alpha_{\rm D}$ is proportional to $\alpha_{\rm D}^{-1/2}$. Therefore, for small $\alpha_{\rm D}$, the NA64 constraints on ϵ^2 are stronger.

[18] Here, we consider the case $m_{Z'} > 2m_\chi$.

[19] The mean free path of a dark photon and LDM particles is proportional to the factor ϵ^{-2}, in contrast to the mean free path of a photon, because the corresponding cross sections of a dark photon (LDM particles) with particles of our matter are suppressed by the factor ϵ^2. With $\epsilon = 10^{-3}$ and the photon mean free path 5 mm, we obtain a dark photon mean free path of the order of $O(10^4)$ meters. A similar estimate is also applicable to LDM particles. Therefore, dark photons and LDM particles pass through matter in the detector freely, quite similar to neutrinos.

We note that another advantage of NA64 is that the experiment is largely model-independent, because it has no essential sensitivity either to the spin of the A′ boson or to the details of its invisible decay. The only assumption that is made is a nonzero coupling of A′ to the electron and the dominance of the A′-boson decays into invisible modes. When a signal is detected (the number of events with a nonzero missing energy exceeds the background level), it can be unambiguously asserted that the experiment yields evidence in favor of the existence of new light penetrating particles. In the model with the A′ boson decaying into invisible modes, it is then possible to estimate the A′ mass based on the shape of the missing energy spectrum [73].

The NA64 experiment can also be used to search for visible $A' \to e^-e^+$ decays. For that, the installation involves not one calorimeter, as in the search for invisible decay modes of A′, but two electromagnetic calorimeters: WCAL (Wolfram CALorimeter) and ECAL. The incident electron hits the first calorimeter, WCAL, where an A′ is produced that then decays outside the WCAL. Products of the $A' \to e^-e^+$ decay are detected in the second ECAL located downstream along the beam. The signature of such a reaction is that the sum of the energies released in the WCAL and ECAL equals the energy of the initial electron, $E_e \approx E_{WCAL} + E_{ECAL}$, which makes it possible to strongly suppress the background (see Section 3.3).

3.2 NA64 experiment with an electron beam. Invisible mode

In the NA64 electron experiment, an optimized 100-GeV electron beam of the H4 channel in the northern zone of the SPS at CERN is used, as is described in detail in [37]. An electron beam is generated by irradiating a beryllium target with a primary proton beam with a momentum of 400 GeV/c and intensity up to several trillion (10^{12}) protons on target (POT) in one shot with a duration of 4.8 s and the number of dumps from 1 to 4 per minute, depending on the operating mode of the accelerator. Short-lived neutral pions produced in proton collisions decay inside the target into two gamma quanta with the subsequent conversion of the decaying gamma quanta into e^+e^- pairs inside a thin lead converter. Protons and charged secondary particles that did not interact in the converter are deflected by a strong magnetic field and are directed to the absorber. The electrons (positrons) resulting from the conversion enter the NA64 detector via an evacuated channel tuned to a specific (adjustable) beam momentum. The channel ensures an ultrapure electron beam with a maximum intensity up to 10^7 electrons per dump in the range of momenta from 50 to 200 GeV/c. The admixture of hadrons (mostly pions) in the electron beam is $\pi/e^- \lesssim 10^{-2}$. The beam has a transverse size of the order of 1 cm^2 and a halo with an intensity of several percent of the main beam intensity.

Figure 2. Photo of the NA64 detector.

Detection of signal events in NA64 is based on the high purity and reliable identification of incoming electrons and measurement of their energy in the initial and final states, because the product of the $A' \to$ invisible decay is not detected. The NA64 detector shown in Fig. 2 is located at a distance of about 500 m from the proton target. The installation is outlined in Fig. 3. The installation involves scintillation (Sc) counters S1–S3 and a veto counter V1 to separate the primary beam, as well as a spectrometer consisting of two successive dipole magnets with the integrated field $\simeq 7$ T m and a tracker with a small amount of matter in the beam for precision measurement of the momentum of incoming particles. The tracker is a set of planes T1–T4 of various chambers located before the magnets (T1, T2) and after the magnets (T3, T4) and measuring the momentum P_e of the incoming e^- with the accuracy $\delta P_e/P_e \simeq 1\%$.[20]

To improve the selection of electrons with an energy of 100 GeV and to suppress the background from possible contamination with low-energy particles, a tagging system was utilized that uses synchrotron radiation (SR) of the incoming electrons in a magnetic field. Because the SR

[20] MicroMegas [74], GEM, and Straw Tube (ST) [75] type chambers were used in the experiment.

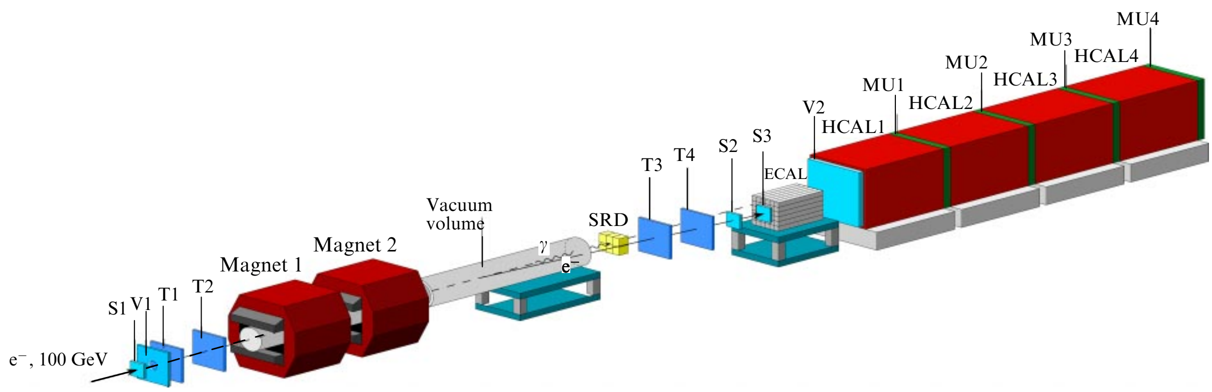

Figure 3. (Color online.) Schematic of the NA64 unit for the search for invisible decays of A′ bosons produced in the reaction $eZ \to eZA'$ of bremsstrahlung radiation of incident electrons with nuclei of the active ECAL target.

energy of a particle with a mass m and energy E_0 is $\langle E_{\mathrm{SR}} \rangle \propto E_0^3/m^4$, the contamination of the beam by electrons and low-energy hadrons can be effectively suppressed by setting the threshold for the energy released in the synchrotron radiation detector (SRD) [62, 76]. For this, a vacuum volume approximately 15 m in length was placed between the magnets and the target (ECAL) in order to minimize the absorption of SR photons detected directly in the lower beam part of the volume using the SRD, which is a compact lead-scintillation (PbSc) sandwich calorimeter with fine longitudinal segmentation. The detector is also divided laterally into three independent counters. The use of transverse SRD segmentation allows additionally suppressing the background coming from beam hadrons that could trigger SRD (tagging electrons) as a result of knocking out energetic delta-electrons from the exit window of the vacuum volume, by about two orders of magnitude [76].

The detector is also equipped with an active target, which is a hodoscopic ECAL for measuring the energy E_{ECAL} of electrons in the final state with the accuracy $\delta E_{\mathrm{ECAL}}/E_{\mathrm{ECAL}} \simeq 0.1/\sqrt{E_{\mathrm{ECAL}}[\mathrm{GeV}]}$, as well as the X and Y coordinates of incoming electrons using the transverse profile of an electromagnetic shower. The ECAL length is about 40 radiation absorption lengths X_0, with the initial section of about 4 X_0 used as a prestorm (PS) detector. The requirement that the signal be present in all three SRD counters, combined with the use of information on the longitudinal and transverse development of the electromagnetic shower in the ECAL, allows suppressing the initial level of the hadron contamination of the beam by more than four orders of magnitude, while maintaining the efficiency of electron identification at a level exceeding 95% [76].

A high-performance veto counter V_2 and a massive sealed HCAL with a total thickness of approximately 30 nuclear interaction lengths (λ_{int}), placed immediately after the ECAL, are used to reject nuclear interactions events of incoming electrons in the target. The HCAL is a set of four independent modules HCAL1–HCAL4 and muon counters MU1–MU4 and also serves to efficiently identify muons.

3.2.1 Data analysis and background. The analysis described below involves a dataset with the total number of electrons on target (EOT) $n_{\mathrm{EOT}} = 2.84 \times 10^{11}$, obtained in 2016–2018 on a 100-GeV electron beam with an intensity up to 9×10^6 electrons per dump. Here, we briefly describe the procedure for selecting and analyzing data; a more detailed description can be found in [39]. To avoid bias in determining the selection criteria for candidates for signal events, a blind analysis was carried out. It was assumed in selecting that the missing energy should be $E_{\mathrm{miss}} = E_0 - E_{\mathrm{ECAL}} > 50$ GeV. The signal domain ($E_{\mathrm{ECAL}} < 50$ GeV, $E_{\mathrm{HCAL}} < 1$ GeV) was determined based on calculations of the energy spectrum of A′ bosons emitted by $e^{\pm}$ from the electromagnetic shower generated by the primary electron in the target and on measurements of the HCAL noise level directly in the experiment [39, 61, 73].

Monte Carlo (MC) simulations using the Geant4 software package [77], used to study the detector response, the signal recovery efficiency, and the background level, together with the analysis procedure, including selection criteria and sensitivity assessment, are described in detail in [39]. The differential cross section of A′ production in reaction (13) can be calculated using the IWW approximation [59] (see also [60, 61]). These cross sections were used to simulate the A′ production process using the DMG4 package [78], fully compatible with Geant4 [77], which was used to evaluate the detector response.[21] The total number $n_{\mathrm{A}'}$ of produced A′ bosons per electron depends, in particular, on the parameters ϵ, $m_{\mathrm{A}'}$, and E_0 and can be calculated as

$$n_{\mathrm{A}'}(\epsilon, m_{\mathrm{A}'},\, E_0) = \frac{\rho N_{\mathrm{A}}}{A_{\mathrm{Pb}}} \sum_i n(E_0, E_{\mathrm{e}}, s)\, \sigma^{\mathrm{A}'}_{\mathrm{IWW}}(E_{\mathrm{e}}) \Delta s_i\,, \quad (48)$$

where ρ is the target density, N_{A} is Avogadro's number, A_{Pb} is the atomic mass of Pb, $n(E_0, E_{\mathrm{e}}, s)$ is the number of $\mathrm{e}^{\pm}$ with the energy E_{e} in an electromagnetic shower at a depth s (expressed in radiation lengths) inside a target with the total thickness T, and $\sigma^{\mathrm{A}'}_{\mathrm{IWW}}(E_{\mathrm{e}})$ is the IWW approximation of the cross section of A′ production by an electron with the energy E_{e} in the reaction $\mathrm{eZ} \to \mathrm{eZA}'$ in the kinematically allowed region up to $E_{\mathrm{A}'} \simeq E_{\mathrm{e}}$. The energy distribution $\mathrm{d}n_{\mathrm{A}'}/\mathrm{d}E_{\mathrm{A}'}$ of A′ was calculated using the differential cross section $\mathrm{d}\sigma(E_{\mathrm{e}}, E_{\mathrm{A}'})/\mathrm{d}E_{\mathrm{A}'}$ based on the results in [73]. Numerical summation in Eqn (48) included a detailed modeling of electromagnetic showers, taking the A′ energy spectrum in the target into account.

It was noted relatively recently that, for a certain kinematic range of the parameters $m_{\mathrm{A}'}$ and $E_{\mathrm{A}'}$, the yield of A′ obtained within the IWW approximation can differ significantly from that obtained by accurate calculations at the tree level [60, 61]. A reliable theoretical estimate of the yield of A′ is required both for the correct interpretation of experimental results and for obtaining reliable constraints in the A′ parameter space or for possible observations of the A′ signal. We therefore performed calculations of the A′ production cross section by exactly integrating the phase space over final-state particles in the reaction $\mathrm{e^-Z} \to \mathrm{e^-ZA}'$, which reduces to the replacement $\sigma^{\mathrm{A}'}_{\mathrm{IWW}}(E_{\mathrm{e}}) \to \sigma^{\mathrm{A}'}_{\mathrm{exact}}(E_{\mathrm{e}})$ in formula (48). Here, $\sigma^{\mathrm{A}'}_{\mathrm{exact}}(E_{\mathrm{e}})$ is the exact value of the cross section at the tree level.

In Fig. 4a, we show the distribution of approximately 3×10^4 events from the reaction $\mathrm{e^-Z} \to$ anything in the $E_{\mathrm{ECAL}} - E_{\mathrm{HCAL}}$ plane derived from combined data at an earlier stage of the analysis using soft selection criteria, which mainly require the presence of an input track identified as an electron in the SRD. Events in domain I correspond to the production of dimuons due to the dominant quantum electrodynamics process $\mathrm{e^-Z} \to \mathrm{e^-Z}\gamma$, $\gamma \to \mu^+\mu^-$ of the conversion of hard bremsstrahlung photons on a target nucleus, which is characterized by an energy of the order of 10 GeV released by a pair of dimuons in HCAL modules. This rare process has been taken as a reference that allowed validating the reliability of MC simulations, correcting signal acceptance, cross-validating systematic uncertainties, and estimating the background [39]. Domain II corresponds to hadron electroproduction events in the target that satisfy the energy conservation $E_{\mathrm{ECAL}} + E_{\mathrm{HCAL}} \simeq 100$ GeV within the energy resolution of the detectors.

Finally, in order to maximize the output of signal events with a minimal background, the following selection criteria were used:

(1) the momentum of the incoming electron track must be within 100 ± 3 GeV;

(2) the SRD energy must be in the SR energy range of electrons in magnets and coincide in time with the trigger;

[21] About 10^{10} events have been simulated. Many background processes, for example, decays of pions and kaons and hadron interactions in the target, were simulated with the actual statistics or were evaluated directly from the data.

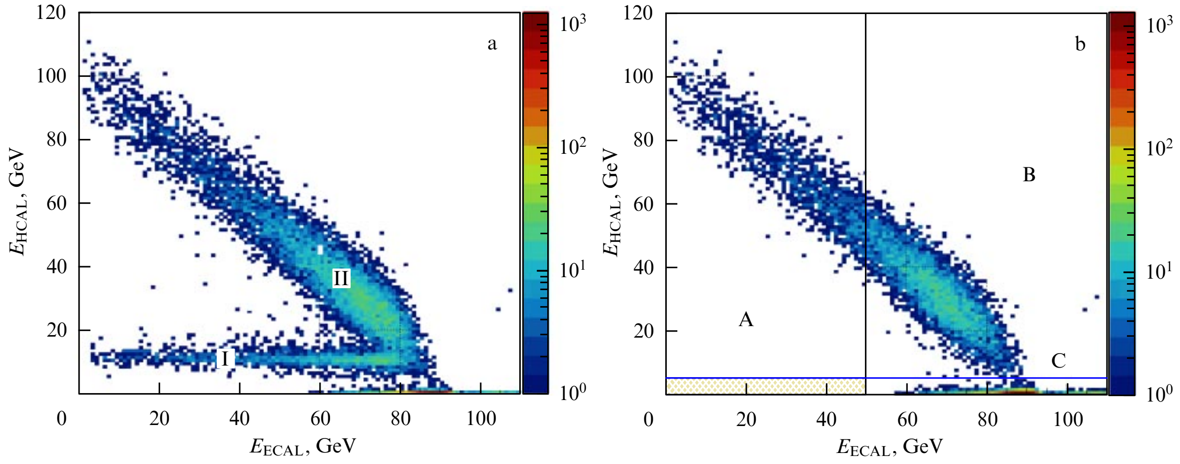

Figure 4. (Color online.) (a) Measured distribution of events in the ($E_{\rm ECAL}, E_{\rm HCAL}$) plane obtained from combined data at an early stage of analysis. (b) The same distribution after the use of all the selection criteria. Hatched part shows the signal domain, which contains no events. The efficiency of detection of A$'$ in the signal domain is $\simeq 50\%$. The size of this domain along the $E_{\rm HCAL}$ axis is enlarged by a factor of five for visual clarity. Extrapolation from domains A and C is used to estimate the background inside the signal domain.

(3) the transverse and longitudinal shape of the shower in the ECAL must correspond to that expected from a signal shower;

(4) in the tracker cameras, there must be only one track in front of the target in order to suppress the background from interactions with channel matter in the absence of activity in the veto counters.

Among all the data, about 1.6×10^4 events met these criteria.

The main background in the search for A$'$ arises from the production of hadrons in the interaction of the e^- beam in matter of the lower part of the channel. In rare cases, these reactions are accompanied by the emission of a soft electron accompanied by secondary hadrons escaping at large angles. Such events can simulate a signal due to the insufficient air-tightness of the detector. This background coming from charged secondary particles was largely suppressed by the requirement that additional tracks (or hits) be absent in the T3 chambers (mainly a Straw Tube, located after the magnets), which have the greatest lateral acceptance in the installation. Also required was the presence of one track and the absence of additional hits in the chambers located before the magnets. The remaining background from wide-angle neutral hadrons was largely estimated directly from the data by extrapolating events from the neighboring regions ($E_{\rm ECAL} > 50$ GeV, $E_{\rm HCAL} < 1$ GeV) to the signal region, taking systematic errors into account and varying the shape functions chosen for extrapolation, as described in [39]. The shape of the extrapolation functions was estimated based on the study of a statistically significant set of events from hadronic interactions of electrons in the target and their independent verification by simulation.

Another background from leading neutral hadrons (with energies exceeding $0.5\,E_0$) $(\mathrm{n}, \mathrm{K}_L^0)$ penetrating without interaction and produced in the interactions of electrons in the target was studied using events from the region ($E_{\rm ECAL} < 50$ GeV, $E_{\rm HCAL} > 1$ GeV), which were purely neutral events generated in the ECAL that have passed the veto-counter selection. The level of this background, which was estimated from data using longitudinal segmentation of the HCAL and a conservative estimate of the probability of penetration, was found to be small. Several other background sources that can simulate a signal, such as the loss of dimuons due to statistical signal fluctuations or muon decays, flight decays, and beam π and K mesons erroneously tagged by the SRD, have been simulated with the full data statistics and also turned out to be negligible. Estimates of the main backgrounds [39] corresponding to the statistics $N_{\rm EOT} = 2.84 \times 10^{11}$ are given in the table.

3.2.2 Constraints on the $\gamma - \mathrm{A}'$ mixing parameter ϵ and on LDM parameters. A thorough analysis of the background outside the signal area, carried out using the selection criteria described in Section 3.2.1, allowed suppressing its main sources and verifying that the expected background in the signal area is at the level of 0.5 events (see the table). As shown in Fig. 4b, no events were detected after opening the signal area. This allowed obtaining new upper bounds for the mixing parameter depending on the mass $m_{\mathrm{A}'}$.

In the final procedure for obtaining constraints from the 2016–2018 session data, statistical analysis was used based on the RooStats package [79]. The background estimation, signal efficiency, and their corrections and uncertainties were used to optimize the main threshold for $E_{\rm ECAL}$, which defines the signal area. This was done by comparing them with the sensitivity, defined as the mean expected bound calculated using the profile likelihood method depending on $E_{\rm ECAL}$. The calculations were carried out with uncertainties used as error parameters, assuming their log-normal distributions.

The combined bounds for $\gamma - \mathrm{A}'$ mixing at a 90% confidence level (CL) depending on the A$'$ mass, calculated

Table. Expected background for 2.84×10^{11} EOT.

	Background source	Background, $n_{\rm b}$
1	Dimuons	0.024 ± 0.007
2	π, K $\to$ eν, K$_{e3}$ decays	0.02 ± 0.01
3	Nonhadronic interactions of electrons on the beam line material	0.43 ± 0.16
4	Hadronic interactions of electrons in the target	< 0.044
5	Photons penetrating the HCAL without interactions	< 0.01
Total $n_{\rm b}$ (conservative value)		0.53 ± 0.17

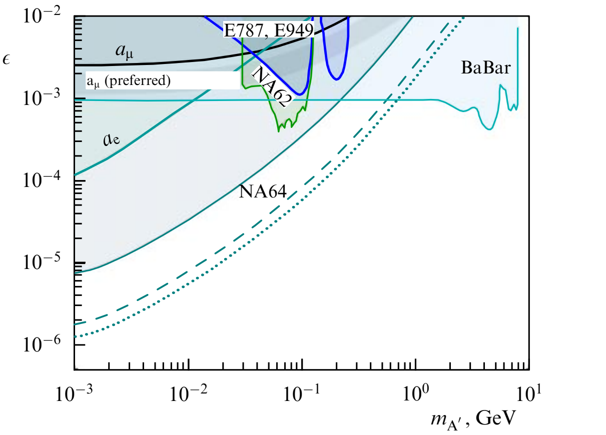

Figure 5. (Color online.) NA64 exclusion domain at the 90% CL (area bounded by the curve marked as NA64) in the parameter plane $m_{A'} - \epsilon$. Also shown are the constraints obtained in the E787 and E949 [16, 158] and BaBar [159] experiments, recent NA62 results [160], and constraints resulting from the anomalous magnetic moment of the electron a_e and the muon a_μ. In addition, the expected NA64 constraints are presented under the assumption of no backgrounds and $N_{EOT} = 5 \times 10^{12}$ (dashed line) and $N_{EOT} = 10^{13}$ (dotted line). In the range $m_{A'} < 1$ MeV, the constraints on ϵ resulting from astrophysical and cosmological data are much stronger, because obtaining reliable experimental restrictions in this area requires a more thorough analysis of the propagation of light A′ in matter (see, e.g., [161]). The range $\epsilon \gtrsim 10^{-2}$ is bounded by the contributions of A′ to a_e and a_μ.

with the expected backgrounds and estimated systematic errors taken into account, are shown in Fig. 5. At present, the constraints in [40] are the best for the mass range $0.001 \lesssim m_{A'} \lesssim 0.2$ GeV among those obtained in direct searches for the $A' \to$ invisible decay [15]. Bounds for the mixing parameter ϵ expected in the electron-beam NA64 experiment at $N_{EOT} = 5 \times 10^{12}$ and $N_{EOT} = 10^{13}$ are shown in Fig. 5 by the respective dashed and dotted lines.[22]

To assess the sensitivity of the NA64 experiment to the search for LDM [80], formulas in Section 2 were used to predict the dependence of ϵ^2 on α_D, m_χ, and $m_{A'}$ under the assumption that the LDM was in thermodynamic equilibrium with the observable matter in the early Universe. For specific calculations, the values $\alpha_D = 0.02$, 0.05, and 0.1 and $m_{A'}/m_\chi = 2.5$, 3 were taken. The calculations were carried out for scalar, Majorana, and pseudo-Dirac ($\delta \ll 1$) DM.

The main conclusion in [80] is that, for $N_{EOT} = 5 \times 10^{12}$, NA64 will be able to eliminate the scalar and Majorana LDM models for $\alpha_D \leqslant 0.1$ and $m_{A'}/m_\chi \geqslant 2.5$ in the A′ mass range $1 \leqslant m_{A'} \leqslant 60$ MeV. Pseudo-Dirac LDM can also be ruled out by NA64 for $\alpha_D \leqslant 0.05$ and $m_{A'}/m_\chi \geqslant 3$. As follows from [80], NA64 with the statistics $N_{EOT} = 2.84 \times 10^{11}$ has already ruled out the scalar LDM model with $\alpha_D \leqslant 0.05$ and $m_{A'}/m_\chi \geqslant 3$ and the Majorana LDM model with $\alpha_D = 0.02$ and $m_{A'}/m_\chi \geqslant 3$ for the A′ mass in the range of 1–200 MeV. The implications of the results obtained by NA64 in the form of constraints on the parameters of LDM models with a vector mediator are also shown in Fig. 6. We note that the assumption that the LDM models give a correct prediction of DM density leads to a prediction of the product $\alpha_D \epsilon^2$ as a function of the masses of the mediator and LDM particles (see Section 2.5). Because experiments such as NA64 and BaBar yield the upper bound on mixing parameter ϵ, it is much more difficult to exclude LDM models for large than for small α_D.

3.2.3 Resonance domain problem. The LDM particle annihilation cross sections in (36) and (40) are proportional to the factor $K = \epsilon^2 \alpha_D (m_{A'}^2/m_\chi^2 - 4)^{-2}$. From the assumption that DM particles were in thermodynamic equilibrium with SM matter particles in the early Universe, we can predict the dependence of K on the mass m_χ of LDM particles (see Section 2.5). In the resonance domain $m_{A'} \approx 2m_\chi$, the parameter ϵ^2 is proportional to the factor $(m_{A'}^2/m_\chi^2 - 4)^2$, which allows decreasing the predicted value of ϵ^2 by 2 to 4 orders of magnitude [81], in comparison with that in the often-studied case $m_{A'}/m_\chi = 3$. This means that the NA64 experiment, as well as other planned experiments, will not be able to fully test the resonance domain $m_{A'} \approx 2m_\chi$. We note that the values of $m_{A'}$ and m_χ are arbitrary, and therefore the case where $m_{A'} \approx 2m_\chi$ can be regarded as a fitting of the parameters. It is natural to require the absence of significant parameter fitting. We therefore assume that $m_{A'}/2m_\chi - 1 \geqslant 0.25$, i.e., $m_{A'} \geqslant 2.5 m_\chi$. As follows from the results in [80], NA64 is able to test the most interesting scenarios where $m_{A'} \geqslant 2.5 m_\chi$ with $N_{EOT} = 5 \times 10^{12}$.

3.3 Search for visible decays A′, X(17) → e⁺e⁻ of hypothetical particles in the NA64 experiment

In the Atomki experiment [82], a 6.8σ excess was observed of events in the invariant mass distribution of e^+e^- pairs produced in nuclear transitions of excited beryllium $^8Be^*$ to the ground state via the creation of an electron-positron pair. This anomaly can be explained, for example, as a result of the emission of a new X boson with a mass of 16.7 MeV, followed by its decay $X \to e^+e^-$ under the assumption that the X boson has nonuniversal coupling constants with quarks and leptons in the range $2 \times 10^{-4} \lesssim \epsilon_e \lesssim 1.4 \times 10^{-3}$, and its lifetime is $10^{-14} \lesssim \tau_X \lesssim 10^{-12}$ s [83]. The results of the Atomki experiment greatly enhanced interest in theoretical and experimental studies on the search for new light bosons and investigations of their properties (see [84–90]). Another strong motivation for the search for a new light boson decaying into an e^+e^- pair is associated with the hypothesis of the existence of LDM.

A method for searching for the $A' \to e^+e^-$ decay was proposed in [62]. It is also applicable in the case of the $X(17) \to e^+e^-$ decay. Briefly, a high-energy electron beam is directed into an electromagnetic calorimeter, which serves as an active target. Usually, a beam electron loses all of its energy in the target due to the complete absorption of the electromagnetic shower generated by it. If the A′ (or X(17)) boson exists, then it must sometimes be produced by a shower electron (or positron) due to the A′(X(17))–e⁻ coupling as a bremsstrahlung particle in the scattering of an electron (positron) on target nuclei:

$$e^- + Z \to e^- + Z + A'(X(17)), \quad A'(X(17)) \to e^+e^- . \tag{49}$$

Because the A′ boson is a weakly interacting particle, it leaves the target without interaction and can subsequently decay into an e^+e^- pair outside the target before the next downstream ECAL. In this case, it is assumed that A′ is a relatively long-lived particle with a decay length L_d (see Section 2.3.1)

[22] In obtaining the expected bounds, the absence of background events for $N_{EOT} = 5 \times 10^{12}$ and $N_{EOT} = 10^{13}$ is assumed. This assumption is based on simulations of the background using data obtained with the use of the new wide-aperture HCAL in an upgraded NA64 installation to suppress the background coming from hadrons with large transverse momenta.

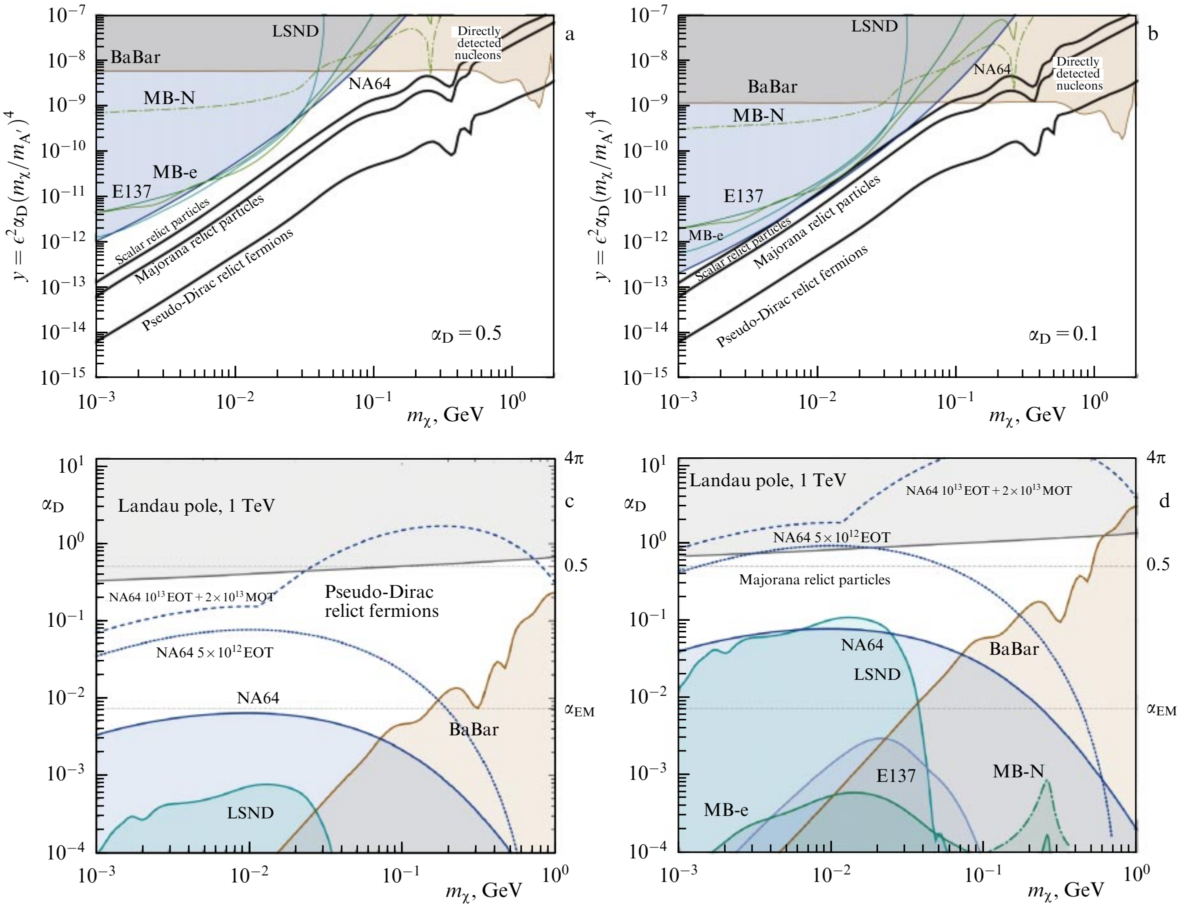

Figure 6. (Color online.) NA64 bounds on the (y, m_χ) plane obtained at (a) $\alpha_D = 0.5$ and (b) $\alpha_D = 0.1$ from complete 2016–2018 dataset. The regions above the curves on which the observed LDM density is realized correspond to a low density of LDM, and the regions below those curves, to a high LDM density. NA64 constraints in the plane (α_D, m_χ) for (c) pseudo-Dirac and (d) Majorana LDM types, obtained under the assumption that the parameters of the models correspond to the observed DM density in the present-day Universe. Areas below NA64 curves are excluded. Constraints are shown in comparison with estimates obtained in [5–8, 16, 162, 163] from results of LSND [164, 165], E137 [166], MiniBooNE MB-e and MB-N [167], BaBar [159], and experiments on direct search for LDM [168]. Preferred parameters explaining the observed density of relict LDM for scalar, pseudo-Dirac, and Majorana LDM particles are shown by solid curves in Figs a and b (see, e.g., [11]). Also shown are combined bounds from NA64e and NA64μ with $N_{EOT} = 10^{13}$ plus $N_{MOT} = 2 \times 10^{13}$ (dashed line) obtained under the assumption of a negligibly small background.

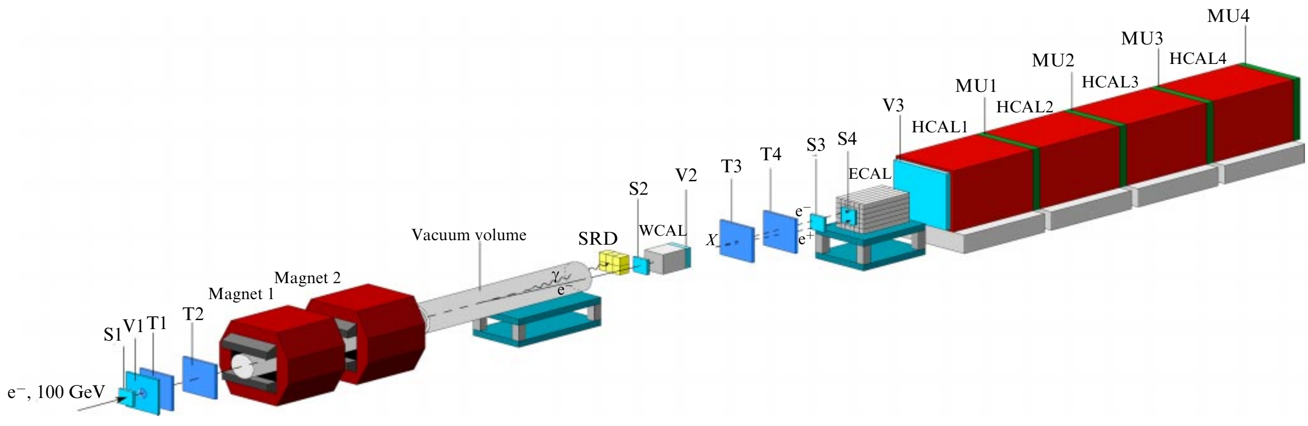

Figure 7. (Color online.) Schematic of the NA64 setup for the search for visible $A' \to e^+e^-$ decays resulting from the $eZ \to eZA'$ reaction of an incident electron with an active WCAL target.

not too short compared to the target length L_t, such that the probability of A' leaving the target is at least 10%. The $A'(X(17)) \to e^+e^-$ decay signature is therefore an event with two electromagnetic showers in the detector: one shower in the target and the other in the next ECAL, with the sum of the energies equal to the beam energy.

The NA64 setup is shown schematically in Fig. 7. The experiment involves an optimized electron beam with an energy of 150 GeV of the H4 channel in the northern zone of an SPS accelerator. The setup is identical to the one described above for searching for $A' \to$ invisible decays (see Section 3.2) except for using an additional WCAL electromagnetic calorimeter as an active target for the production of A′, X(17) [37, 62]. WCAL is a compact tungsten calorimeter for increasing the sensitivity of searches for short-lived A′ and X(17). Placed next after the WCAL is the ECAL electromagnetic hodoscopic calorimeter, at a distance of about 3.5 m, which serves to measure the energy of the e^+e^- decay pair. The results presented in Section 3.3.1 were obtained from data corresponding to 2.4×10^{10} and 3×10^{10} electrons on WCAL targets of the respective lengths $40\,X_0$ (290 mm) and $30\,X_0$ (220 mm). The data from these two sessions were analyzed using similar selection criteria and combined taking the appropriate normalization into account.

3.3.1 Data analysis and the background. Candidate events were selected using criteria that maximize signal performance with minimal background levels. The criteria were selected based on both the simulation of the setup using Geant4 [77] and the use of part of the data. According to the simulation results, at least 30% of the total energy must be released by signal events in the ECAL [61, 73].

As in the previous cases [38–40], a pure sample of about 10^5 rare events of $\mu^+\mu^-$ produced in the WCAL target was used to correct the efficiency in the simulation. We also analyzed the data with the choice of the signal region $90 < E_{\rm tot} < 110$ GeV and the use of 20% (100%) data to optimize the selection criteria (to estimate the background).

The most important background source was the decay chain $K^0_S \to \pi^0\pi^0, \pi^0 \to \gamma e^+e^-$ from the leading K^0_S produced in the WCAL and the photon conversion $\gamma \to e^+e^-$ from the chain $K^0_S \to \pi^0\pi^0 \to \pi^0 \to \gamma\gamma$ on the channel material, for example, in a T3 chamber. Another source of the background, related to hadronic decays $K^0_S \to \pi^+\pi^-$ that could be erroneously identified as an electromagnetic shower in the ECAL at a level below 2.5×10^{-5}, was estimated from the results of measurements made with a pion beam. After determining and optimizing the selection criteria and evaluating the background levels, the signal region was explored in NA64, and no candidates for $A', X(17) \to e^+e^-$ decays were found.

The NA64 constraints [41] on the ϵ parameter as a function of the A′-boson mass, together with the results of other experiments, are shown in Fig. 8. The NA64 results exclude the X boson as an explanation for the ^{8}Be* anomaly for the X–e$^-$ coupling constant $\epsilon_e \lesssim 6.8 \times 10^{-4}$ for the mass $m_X = 16.7$ MeV, while leaving the parameter region $6.8 \times 10^{-4} \lesssim \epsilon_e \lesssim 1.4 \times 10^{-3}$ open to future searches, which seem extremely interesting. A further increase in sensitivity in the region of large X–e$^-$ coupling constants is limited by a decrease in the X boson lifetime with increasing ϵ_e, $\tau_X \sim 1/\epsilon_e^2$, which results in decreasing the probability of its escape from the target, proportionally to $\exp(-L_t/L_d)$ (where $L_d \sim E_X/\epsilon_e^2$). It follows that moving into this region requires both a decrease in the target length L_t and an increase in the beam energy [91].

We note that the Atomki collaboration recently reported an observed similar excess of events with approximately the same invariant mass in nuclear transitions involving another nucleus, ^{4}He [92]. This sharply raises the importance of confirming the observed excess of events by other nuclear physics experiments, as well as by particle physics experiments on independent searches for the X boson. To study the remaining range of parameters corresponding to a short-lived X boson with lifetime $\tau_X \lesssim 10^{-13}$ s, the installation has to be significantly upgraded with a new high-precision tracker and magnetic spectrometer, providing the possibility of also reconstructing the invariant mass of the e^+e^- pair for unambiguous detection of the X boson [91].

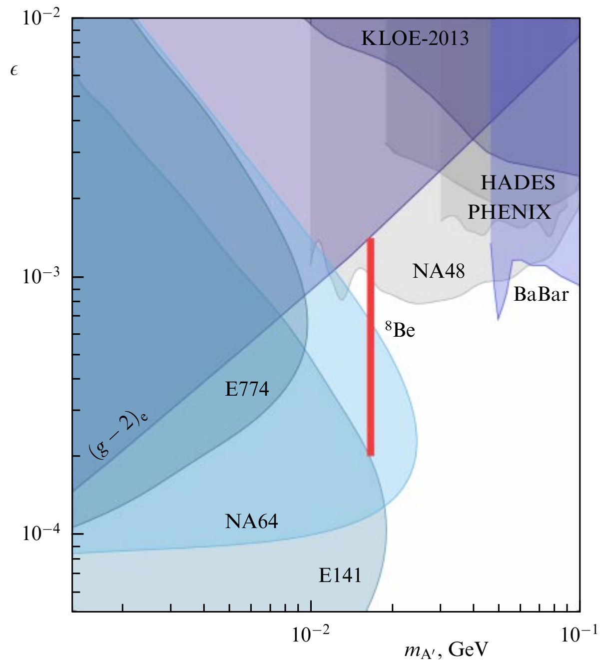

Figure 8. (Color online.) Domain excluded at a 90% CL level in the plane $m_{A'(X17)} - \epsilon$ according to the NA64 experiment (blue region). For a mass of 16.7 MeV, NA64 excludes the domain of (X, e^-) coupling constants in the range $1.2 \times 10^{-4} < \epsilon_e < 6.8 \times 10^{-4}$. The total admissible range of values of ϵ_e explaining the ^{8}Be* anomaly, $2.0 \times 10^{-4} \lesssim \epsilon_e \lesssim 1.4 \times 10^{-3}$ [83], is shown with a vertical red bar. Constraints on ϵ obtained in other experiments are also presented (KLOE: K^0_LLOng Experiment, HADES: High Acceptance Dielectron Spectrometer, PHENIX: Pioneering High Energy Nuclear Interaction eXperiment). (From [41].)

3.4 Search for decays of scalar, pseudoscalar, vector, and axial-vector particles

As noted above, it is important to search not only for the LDM particles themselves but also for particles that mediate the coupling of the hidden sector to the SM, especially in the case of the existence of a hidden sector at mass scales up to several GeV.

Most of the research on the NA64 experiment has focused on LDM models based on the vector interaction mediator A′. The analysis shows that the NA64 experiment is sensitive to a much wider class of LDM models and also to the search for light hypothetical particles such as axion-like pseudoscalars or scalars with a photon or electron coupling. A detailed consideration of all the extra possibilities of the NA64 experiment is far beyond the scope of this review. For illustration, we here present recent results of the NA64 experiment on the search for visible and invisible decays of scalar, pseudoscalar, vector, and axial-vector particles.

3.4.1 Search for decays of a scalar and a pseudoscalar into two photons. Neutral scalar (s) or pseudoscalar (a) massive particles are predicted in many extensions of a SM. The most popular light pseudoscalar, the axion, used to solve the *CP*-symmetry conservation problem in strong interactions [93, 94], arises as a consequence of the violation of Peccei–Quinn (PQ) symmetry [95]. Axion-like particles (ALPs)

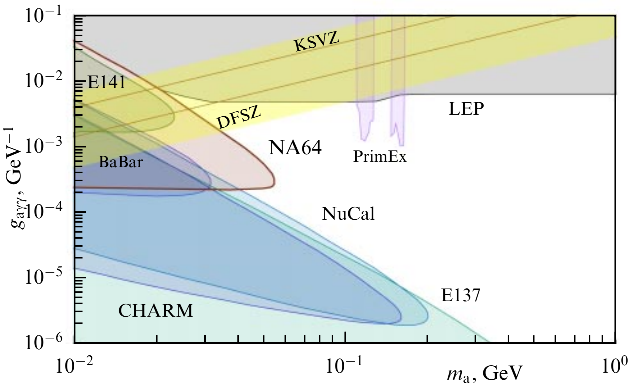

Figure 9. (Color online.) NA64 exclusion domain (darkened region) at a 90% CL for the coupling constant of ALPs coupled mainly to two photons in the $(m_a, g_{a\gamma\gamma})$ plane, as a function of the scalar (pseudoscalar) mass m_a. Yellow band shows the domain of parameters for the leading axion models; constraints from other experiments are also shown (KSVZ: Kim–Shifman–Vainshtein–Zakharov axion model, DFSZ: Dine–Fischler–Srednicki–Zhitnitsky model, PrimEx: Primakoff experiment, LEP: Large Electron Positron collider, CHARM: CERN–Hamburg–Amsterdam–Rome–Moscow collaboration). (From [42].)

that are pseudo-Goldstone bosons arise in models with spontaneously broken PQ symmetry (see, e.g., [96, 97]). This makes ALPs a natural candidate for the role of mediator of a new interaction between the dark and visible sectors, or a candidate for the role of particles of DM itself. ALPs can also explain the discrepancy between theory and experiment for the muon anomalous magnetic moment [64, 98].

The a–$\gamma\gamma$ coupling is determined by the Lagrangian

$$L_{\rm int} = -\frac{1}{4} g_{a\gamma\gamma} F_{\mu\nu} \tilde{F}^{\mu\nu} a\,, \qquad (50)$$

where $g_{a\gamma\gamma}$ is the coupling constant, $F_{\mu\nu}$ is the electromagnetic field strength tensor, and $\tilde{F}^{\mu\nu} = (1/2)\epsilon^{\mu\nu\alpha\beta}F_{\alpha\beta}$ is the dual tensor. Constraints on the ALP in the MeV and GeV ranges were mainly obtained in beam-dump experiments or experiments on e^+e^- colliders [15], and a substantial part of the region, $10^{-4} \lesssim g_{a\gamma\gamma} \lesssim 10^{-2}$ GeV^{-1} in the $(m_a, g_{a\gamma\gamma})$ parameter space, remained unexplored. Theoretical predictions for coupling constants, the mass scale, and ALP decay modes are still rather vague. Therefore, it would be interesting to search for such particles in the above range of masses and coupling constants. One of the possible ways to answer these questions is to search for ALPs in beam-dump experiments. However, for coupling constants in the range $10^{-4} \lesssim g_{a\gamma\gamma} \lesssim 10^{-2}$ GeV^{-1}, such a traditional approach is not promising, because ALPs are expected to be relatively short-lived, decaying mainly inside the beam absorber, in the mass range below 1 GeV.

The NA64 collaboration conducted a model-independent search for light scalar and pseudoscalar ALPs [42] using an SPS electron beam. New particles, if they exist, could be produced as a result of the Primakoff effect when hard bremsstrahlung photons emitted by electrons with an energy of 100 GeV interact in the NA64 active target with virtual photons created by the target nuclei. The produced scalar s and pseudoscalar a would penetrate through the first HCAL module (see Fig. 3) used as protection, and would be observed either via their decay $a(s) \to \gamma\gamma$ in other HCAL modules or as events with a large missing energy, if the decay takes place after passing the HCAL. This method allowed exploring the $(g_{a(s)\gamma\gamma}, m_{a(s)})$ parameter space in a region inaccessible to previous experiments. From the analysis of the data corresponding to 2.84×10^{11} EOT, no evidence of such processes was found [42], which allowed setting new bounds for the a(s)–$\gamma\gamma$ coupling constant depending on the a (s) mass in the energy range below 55 MeV (Fig. 9). Further progress in the mass range $m_{a(s)} > 55$ MeV is limited by a rapid decrease in the lifetime of an ALP with an increase in its mass, $\tau_a^{-1} = g^2_{a\gamma\gamma} m_a^3/(64\pi)$, and hence a rapid decrease in the probability of the ALP decaying outside the HCAL1 module.

3.4.2 Constraints on the invisible scalar, pseudoscalar, vector, and axial vector. Corollaries for $(g-2)_e$. Another category includes NA64 searches for a new dark boson X in the mass range below 1 GeV, which can be a scalar (S), a pseudoscalar (P), a vector (V), or an axial-vector (A) particle [12] weakly coupled to electrons or muons (study of the last option is in progress). To avoid the stringent constraints obtained on the visible decay modes of the light X boson from numerous other experiments [15], it is assumed that the X boson decays predominantly invisibly, i.e., $\Gamma(X \to \text{invisible})/\Gamma_{\rm tot} \simeq 1$, for example, into dark-sector particles.

The e–X coupling with a coupling constant g_X defined as $g_X = \varepsilon_X e$ (where ε_X is a parameter and e is the electron charge) is defined in the S, P, V, and A cases by the phenomenological Lagrangians

$$\begin{aligned} \mathcal{L}_S &= g_S \bar{e} e S\,, \\ \mathcal{L}_P &= i g_P \bar{e}\gamma_5 e P\,, \\ \mathcal{L}_V &= g_V \bar{e}\gamma_\mu e V_\mu\,, \\ \mathcal{L}_A &= g_A \bar{e}\gamma_\mu\gamma_5 e A_\mu\,. \end{aligned} \qquad (51)$$

The NA64 collaboration analyzed data previously used in the search for a dark photon decaying into invisible modes in order to constrain models with axial-vector, scalar, and pseudoscalar mediators [43] and obtained constraints on the coupling constants in these models. The constraints on the corresponding coupling constants $g_A = \epsilon_A e$, $g_S = \epsilon_S e$, and $g_P = \epsilon_P e$ [43] depending on the A$'$ mass are shown in Fig. 10 in the plane (m_X, ε_X). For $m_{A'} \gg m_e$, due to γ_5-invariance, the constraints on $\epsilon_V \equiv \epsilon$ and ϵ_A coincide, as do those on ϵ_P and ϵ_S, and the constraint on ϵ_S is weaker than the corresponding constraint for ϵ by 30%. Thus, NA64 substantially constrained the A$'$-boson coupling constants to the electron for renormalizable models with nonzero coupling constants g_V, g_A, g_S, and g_P.

The appearance of new results [99] on the anomalous magnetic moment of the electron, $a_e = (g-2)_e/2$, stimulated additional interest in the search for new physics in this sector. An ultra-precise experiment performed at the Laboratoire Kastler Brossel (LKB) (France) with rubidium atoms ^{87}Rb reported a new value of the fine structure constant: $\alpha^{-1} = 137.035999206(11)$, measured with a relative accuracy of $81/10^{12}$ [99]. This result improves the accuracy of determining α by a factor of 2.5 compared with previous measurements performed in Berkeley with ^{137}Cs atoms [98], but, surprisingly, significantly differs from the latter, with a difference of 5.4σ. Using these α measurements allows predicting the magnitude of the anomalous magnetic moment of the electron a_e [100], which turns out to be 1.6σ lower and -2.4σ higher than its values $a_e^{\rm exp}$ measured

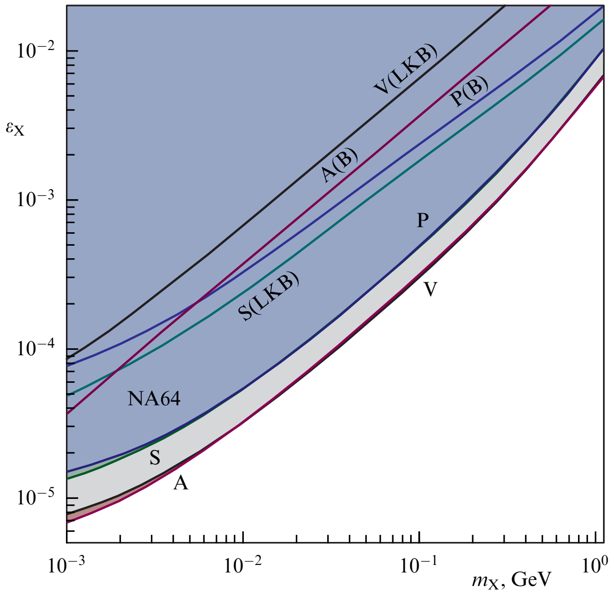

Figure 10. (Color online.) NA64 exclusion domain (hatched area) at a 90% CL in the parameter plane (m_X, ε_X) for vector (V), axial-vector (A), scalar (S), and pseudoscalar (P) X bosons. For comparison, constraints obtained from the results of experiments at the Laboratoire Kastler–Brossel (LKB) [99] and the University of California, Berkeley (Berkeley: B) [98] are also shown.

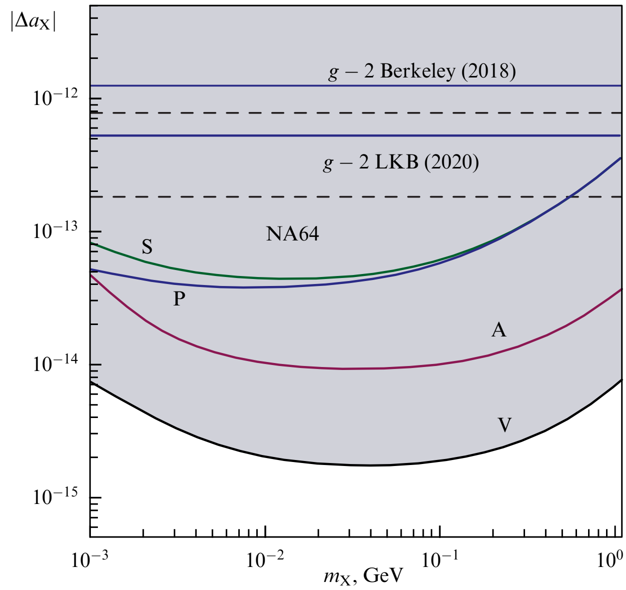

Figure 11. (Color online.) NA64 exclusion domains at a 90% CL in the parameter plane $(m_X, |\Delta a_X|)$ for contributions of S, P, V, and A to a_e (regions above the corresponding curves). For comparison, experimental bounds on the Δa_X values determined by Eqns (52) and (53) are also shown with the respective black dashed and blue solid lines.

respectively at LKB and Berkeley [101]:

$$\Delta a_e = a_e^{\text{exp}} - a_e^{\text{LKB}} = (4.8 \pm 3.0) \times 10^{-13}\,, \tag{52}$$

$$\Delta a_e = a_e^{\text{exp}} - a_e^{\text{B}} = (-8.8 \pm 3.6) \times 10^{-13}\,. \tag{53}$$

The Δa_e errors mainly arise from uncertainties in the measurements of a_e^{exp}. Because the SM predicts a certain value of a_e [100], the results of measurements of this quantity in different experiments should be consistent with each other. With the help of new measurements and improved calculations in the SM, it might be possible to clarify whether the discrepancy between the results in (52) and in (53) is a consequence of still unknown experimental errors or a manifestation of the new physics in $(g-2)_e$ [102]. We note that the result in (53) has already served as a motivation for proposing a number of models aimed mainly at a possible explanation of the discrepancy (53) due to physics beyond the SM (see, e.g., [24, 57, 102–105]).

The results of the NA64 experiment presented above allow estimating the contribution of the new 'dark' boson X to a_e [43]. The corresponding one-loop contributions to $(g-2)_e$ for $m_X \gg m_e$ are [66]

$$\Delta a_S = \frac{g_S^2}{4\pi^2}\left(\frac{m_e}{m_X}\right)^2\left(\ln\frac{m_X}{m_e} - \frac{7}{12}\right), \tag{54}$$

$$\Delta a_P = \frac{g_P^2}{4\pi^2}\left(\frac{m_e}{m_X}\right)^2\left(-\ln\frac{m_X}{m_e} + \frac{11}{12}\right), \tag{55}$$

$$\Delta a_V = \frac{g_V^2}{4\pi^2}\left(\frac{m_e}{m_X}\right)^2\frac{1}{3}\,, \tag{56}$$

$$\Delta a_A = \frac{g_A^2}{4\pi^2}\left(\frac{m_e}{m_X}\right)^2\left(-\frac{5}{3}\right). \tag{57}$$

Given the NA64 constraints on g_V, g_A, g_S, and g_P, we can use formulas (54)–(57) to obtain constraints on the possible contribution of these bosons to the anomalous magnetic moment of the electron [43]. These constraints are in the range $|\Delta a_X| \lesssim 10^{-15}$–$10^{-13}$ for S, P, V, and A with masses in the $\lesssim 1$ GeV region [43]; they are shown in Fig. 11 in the plane $(m_X, |\Delta a_X|)$ together with the experimental constraints on $|\Delta a_X|$ determined by the numerical values in (52) and (53). For small masses $m_X \lesssim 10$ MeV, the bounds for $|\Delta a_X|$ were calculated taking corrections to asymptotic formulas (54)–(57) into account.

The results obtained demonstrate an order-of-magnitude higher sensitivity of the NA64 experiment to probing the new physics than the current accuracy of determining a_e from recent experiments on precision measurements of the fine structure constant and the anomalous magnetic moment of the electron.

3.5 NA64 experiment with a muon beam

As discussed in Section 2.4, if a new vector boson V ($\equiv Z_\mu$) with a mass $m_V \lesssim 1$ GeV exists, weakly coupled mainly to the second and third generations of leptons, then this could explain the muon $(g_\mu - 2)$ anomaly recently confirmed in the E989 experiment at Fermilab. The NA64 collaboration proposed to search for the Z_μ boson in the mass range $m_V \lesssim 2m_\mu$, where it decays mostly in the invisible mode $Z_\mu \to$ invisible, using an M2 SPS muon beam [106, 107]. For example, in the case of a model with the L_μ–L_τ coupling, the invisible decay mode of Z_μ is mainly associated with its decay into two neutrinos, $Z_\mu \to \nu\bar{\nu}$. The proposed extension of the NA64 experiment was named NA64μ. The aim of the experiment in its pilot run in 2021 with a muon beam with the energy $\simeq 100$–160 GeV is to assemble and launch the NA64μ detector and conduct the first search for Z_μ with a coupling constant to the muon in the range $10^{-5} \leqslant g_V \leqslant 10^{-3}$ [107].

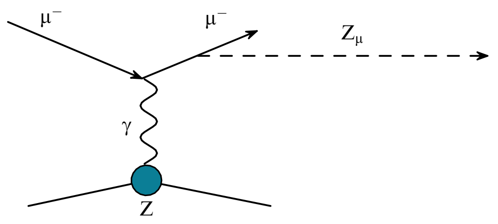

Figure 12. Diagram illustrating the production of a massive Z_μ boson in the reaction $\mu + Z \to \mu + Z + Z_\mu$. The Z_μ boson either is stable or decays in the invisible mode into a pair of neutrinos for $M_{Z_\mu} \leqslant 2m_\mu$ or a $\mu^+\mu^-$ pair for $M_{Z_\mu} > 2m_\mu$.

3.5.1 Search for the Z_μ-boson in the reaction $\mu + Z \to \mu + Z + Z_\mu$, $Z_\mu \to$ invisible. The reaction producing a bremsstrahlung Z_μ boson in the elastic scattering of high-energy muons by a nucleus (Fig. 12)

$$\mu + Z \to \mu + Z + Z_\mu, Z_\mu \to \text{invisible} \qquad (58)$$

is a rare process [108].[23] This reaction is expected at the level $\alpha_V/\alpha \lesssim 10^{-6}$ ($\alpha_V = g_V^2/(4\pi)$) with respect to the level of the usual production of hard photons. This makes the search for the Z_μ boson at this sensitivity level a nontrivial experimental problem.

A schematic view of a setup for searching for the Z_μ boson in reaction (58) is shown in Fig. 13. The detector involves two magnetic spectrometers located before and after the target, designed for independent sequential measurements of momenta of the incoming and outgoing muons and for the precise and reliable identification and reconstruction of the initial and final muon states.

The spectrometer tracking system is a set of Straw Tube ST1–ST4 and ST5–ST8 cameras for measuring the momenta of the respective incident and scattered muons and ST9–ST12 cameras for muon identification. Scintillation counters S1 and S2 are used to determine the small size and divergence of the primary muon beam, and the S3 counter identifies scattered muons and serves to form a trigger. The active target T is surrounded by an ECAL, which, in combination with veto counters V1 and V2, serves as a veto system for identifying the elastic scattering reaction (58) by highly efficient detection of photons and other secondary particles emitted from the target.

Down the beam, the detector is equipped with a highly efficient massive and sealed HCAL located at the end of the device. The HCAL consists of several modules, each of which has transverse and longitudinal segmentation and is mainly used for the effective identification of scattered muons and registration of charged and neutral secondary particles formed during the interaction of primary muons in the target. The central part of the HCAL modules is a cell used to detect scattered muons and secondary particles emitted in the forward direction. The rest of each HCAL module serves to efficiently detect secondary hadrons, electrons, and photons produced in muon interactions $\mu^- Z \to$ anything in the target. The size of the HCAL central cells, track chambers, and S3 counter was determined from a simulation of the setup, including the requirement to effectively register $\gtrsim 90\%$ of scattered muons with a momentum $\gtrsim 30$ GeV. To suppress the background due to ineffective detection of secondary hadrons, the HCAL must be completely sealed in the longitudinal direction. To increase the air-tightness, the selected HCAL thickness is $\simeq (20-30)\lambda_{\rm int}$, where $\lambda_{\rm int}$ is the nuclear interaction length.

The search method with the use of the above-described detector is as follows. The Z_μ (or S) particles[24] are produced as a result of the bremsstrahlung of muons in the reaction $\mu Z \to \mu Z Z_\mu$ (S), which occurs uniformly along the entire length of target T. A fraction (f) of the energy of the primary beam, $E'_\mu = fE_\mu$, is carried away by the scattered muon, which is detected by the second magnetic spectrometer tuned to register momenta $p'_\mu \lesssim f p_\mu$. The rest of the primary muon energy $(1-f)E_\mu$, as a result of the rapid decay $Z_\mu \to$ invisible, is carried away from the installation, resulting in an event with missing energy $E_{\rm miss} = E_\mu - E'_\mu$. An indication of the existence of Z_μ produced in $\mu^- Z$ interactions in the target and decaying in the invisible channel is given by an excess of events with one incoming and one scattered muon, accompanied by an absence of energy release in the detector compared to the expected background.

3.5.2 Background and the expected sensitivity of the experiment. Background sources leading to a signal signature can be classified as follows: (a) physical backgrounds from SM processes due to insufficient air-tightness of the detector; (b) backgrounds associated with the quality of the beam, for example, caused by decays of impurity hadrons in a muon beam; (c) backgrounds associated with measurement errors, for example, of the scattered muon momentum [106, 107]. Exploring these backgrounds down to the $\lesssim 10^{-12}$ level with full-fledged detector simulation would take too much

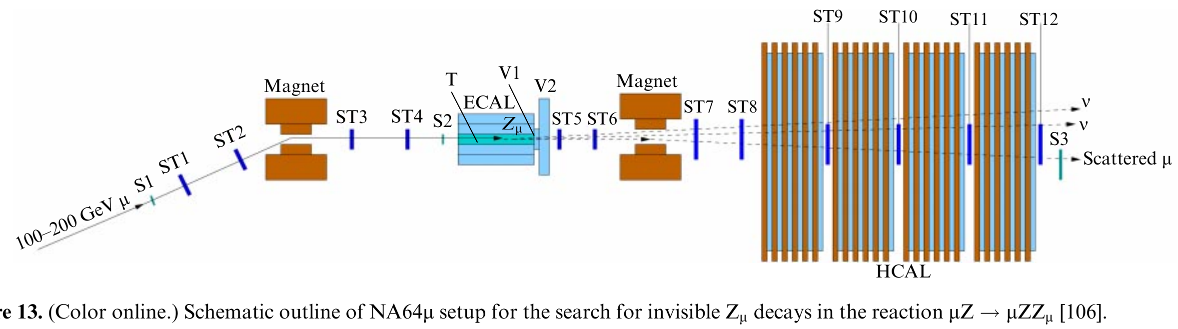

Figure 13. (Color online.) Schematic outline of NA64μ setup for the search for invisible Z_μ decays in the reaction $\mu Z \to \mu Z Z_\mu$ [106].

[23] Z_μ need not necessarily be a vector boson. There are models with a scalar S boson, primarily coupled to the muon.

[24] Here, S is understood as a light scalar particle coupled primarily to the muon and other second- and third-generation quarks and leptons, with the interaction Lagrangian $L_S = g_S \bar{\mu}\mu S$.

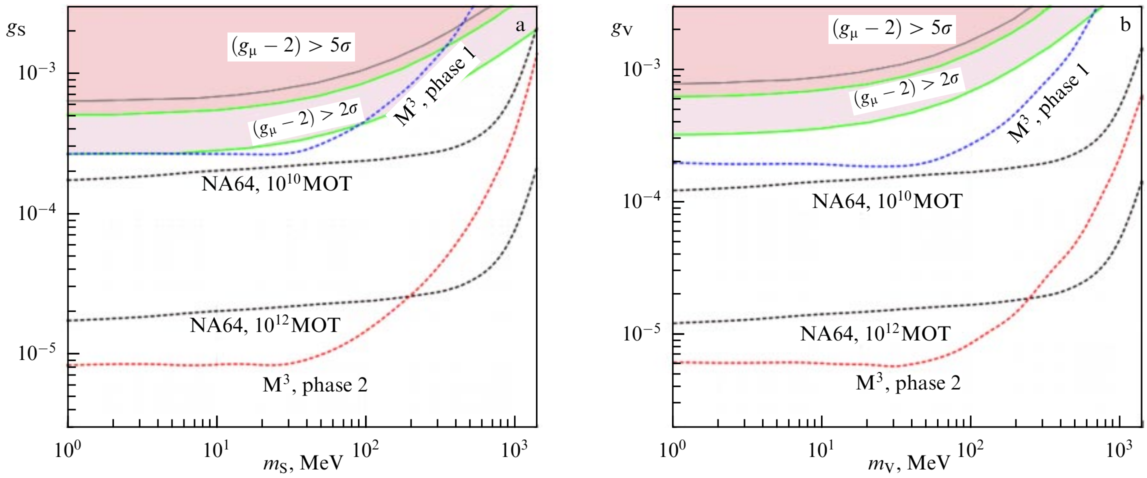

Figure 14. (Color online.) Parameter range for a (a) muon scalar (S) and (b) muon vector (V) particle (see [26, 106, 107]). (a) Expected sensitivity for searching for a dark scalar S in NA64μ experiment [106, 107] under the assumption of the absence of backgrounds and in M^3 FNAL experiment [169]. (b) Expected sensitivity to the vector mediator. It is assumed that S and V decay mostly invisibly. Green curves bound the domain of parameters for which such particles can explain the $(g_\mu - 2)$ anomaly with an accuracy of 2σ. Domains above NA64 curves are expected to be excluded.

computer time. Therefore, only those background sources identified as the most dangerous were considered and evaluated, either using Monte Carlo methods in combination with other numerical calculations or directly from the data of preliminary measurements, as, for example, in the case of evaluating the background from decays of impurity hadrons in a beam or error measurements from the NA64 data obtained with an electron beam. The general background is expected to be $\lesssim 10^{-12}$ [106, 107]. The contribution of additional subdominant background sources (for example, asymmetric decays $\mu \to e\nu\nu$ accompanied by the production of low-energy muons in the HCAL by decay electrons, cosmic muons, etc.) is negligible. This estimate means, for example, that, for $\simeq 10^{12}$ accumulated events, the search for $Z_\mu(S_\mu)$ is expected to be background-free.

To estimate the expected sensitivity, we used the modeling of the Z_μ production process in the detector shown in Fig. 13. Calculations of the production rate and energy distribution of muons produced in SM reactions in the target are based on the results in [109]. The calculated fluxes and energy distributions of scattered muons produced in the target are used to predict the number of signal events in the detector.

Based on the relation $n_{Z_\mu}^{90\%} > n_{Z_\mu}$, where $n_{Z_\mu}^{90\%} = 2.3$ events is the upper bound at 90% CL for the number of signal events, we can estimate the expected constraints of the proposed experiment, which are shown in Fig. 14 together with the values of the coupling constants g_S and g_V needed to explain the $(g_\mu - 2)$ anomaly depending on the Z_μ (or S_μ) mass. These bounds were obtained for the scattered muon energy $10 \lesssim E'_\mu \lesssim 100$ GeV and the efficiency of 50% signal events in the absence of a background for 10^{12} muons on target (MOT) [106, 107]. Within these approximations, the statistical limit of the sensitivity of the proposed experiment is mainly determined by the number of accumulated events.

We note that the experiment described above also allows sensitive searches for A′ bosons with masses $\gtrsim m_\mu$, which makes it possible to test the range of γ–A′ mixing and LDM parameters that is inaccessible to the NA64 experiment on an electron beam, thereby making these experiments complementary to each other [80].

3.6 Combining the results of the NA64e and NA64μ experiments

As we have noted, the expected NA64e and NA64μ bounds for the γ–A′ mixing parameter allow obtaining joint constraints on the LDM model. The annihilation cross section of the LDM particles into observed particles is proportional to the mixing squared, ϵ^2. Therefore, using the constraint on this quantity, we can obtain a constraint in the plane of parameters (y, m_χ), where $y = \epsilon^2 \alpha_D (m_\chi/m_{A'})^4$, and thus constrain the LDM models with the mass $m_\chi \lesssim 1$ GeV. The joint bounds obtained from the data of the 2016, 2017, and 2018 runs and the expected bounds of a future NA64 run are shown in Fig. 6a, b together with the combined NA64e and NA64μ bounds for the respective statistics of 10^{13} EOT and 2×10^{13} MOT [40]. The NA64 results were also compared with those from other experiments.

We emphasize once again that the number of χ particles produced in the NA64 experiment is proportional to ϵ^2, while the corresponding number of signal events in beam-dump experiments is proportional to $\epsilon^4 \alpha_D$. Therefore, for sufficiently small values of α_D, the NA64 bounds for the ϵ^2 parameter are much stronger. This is illustrated in Fig. 6b, where the NA64 bounds are shown for $\alpha_D = 0.1$. It is easy to understand that, for this and smaller values of α_D, the direct search for LDM on NA64e with 5×10^{12} EOT excludes scalar and Majorana LDM models for $m_{A'}/m_\chi = 3$ in the mass range up to $m_\chi \lesssim 0.2$ GeV. At the same time, NA64, in combination with NA64μ, will be able to exclude models with $\alpha_D \leqslant 0.1$ for masses up to $m_\chi \lesssim 1$ GeV. We thus see that, for masses $m_\chi \lesssim 1$ GeV, the joint NA64e and NA64μ constraints are stronger than the bounds obtained from the results of NA64e alone.

4. Other experimental constraints

At present, there are quite a few experimental constraints on models with light A′ bosons. In this section, we briefly mention the most interesting experiments from our point of view and their results.

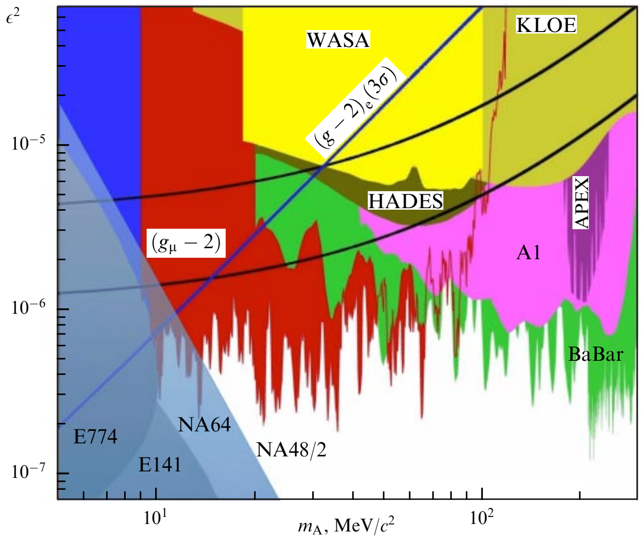

Figure 15. (Color online.) Bounds on the mixing parameter ϵ^2 at a 90% CL depending on the A′ boson mass for visible A′ decays. Color shows excluded domains (WASA: Wide Angle Shower Apparatus). (From [114].)

4.1 Visible A′ decays

4.1.1 Fixed-target electron experiments. Experiments with a fixed target APEX (A Prime EXperiment) [110] at the Jefferson Laboratory and A1 in MAMI (Mainzer Mikrotron, Mainz) [111] used the reaction $e^-Z \to e^-ZA'$ to search for A′ with its subsequent decay into an electron-positron pair, $A' \to e^+e^-$. The absence of a resonance peak in the e^+e^- invariant mass distribution allows obtaining upper bounds on the vector and axial-vector constants $g_{Ve} \equiv \epsilon e$ and $g_{Ae} \equiv \epsilon_{Ae} e$ of the A′-boson coupling to the electron (Fig. 15).[25] The A1 collaboration excluded the parameter domain explaining the $(g_\mu - 2)$ anomaly for masses $50 < m_{A'} < 300$ MeV in the model with a dark photon [111]. At the same time, the APEX collaboration, using an electron beam with the an energy ~ 2 GeV at the Jefferson Laboratory, excluded a similar range of parameters for masses $175 < m_{A'} < 250$ MeV [110].

4.1.2 Electron–positron experiments. The BaBar collaboration at the Stanford Linear Accelerator Center (SLAC) [112] searched for visible decays of A′ bosons in the reaction $e^+e^- \to \gamma A'$, $A' \to l^+l^-$ (where $l = e, \mu$), which manifest themselves as a peak in the invariant mass distribution of the lepton pair l^+l^-. For the model with a dark photon, the mixing parameter $\epsilon \simeq 10^{-2}$–10^{-3} was excluded, depending on the mass in the range $0.212 < m_{A'} < 10$ GeV [112] under the assumption that the visible decays of A′ dominate (see Fig. 15).

The K_L^0 LOng Experiment (KLOE) in Frascati (Italy) searched for A′ in the reactions $e^+e^- \to \Phi \to \eta A' \to \eta e^+e^-$ and $e^+e^- \to \Phi \to \gamma$ $(A' \to \mu^+\mu^-)$ [113]. The constraints obtained are weaker than the corresponding constraints from the NA48/2 [114] and MAMI [111] experiments.

The BaBar collaboration also used the reaction $e^+e^- \to Z'\mu^+\mu^-$, $Z' \to \mu^+\mu^-$ to search for a Z′ boson coupled primarily to a muon. The use of this process allows substantially constraining the coupling constant $g_{V\mu}$ of the Z′ boson to the muon. The results obtained exclude the model with the L_μ–L_τ coupling as an explanation for the $(g_\mu - 2)$ anomaly for $m_{Z'} \gtrsim 200$ MeV [115].

4.1.3 Fixed-target experiments with a proton beam. In the NA-48/2 experiment at CERN, secondary beams of K^+ and K^- were used to search for light A′ bosons in π^0-meson decays [114]. The decays $K^\pm \to \pi^\pm\pi^0$ and $K^\pm \to \pi^0\mu^\pm\nu$ were used to obtain tagged π^0. It was assumed that the source of A′ is the decays $\pi^0 \to \gamma A'$, and the A′ boson itself manifests itself as a narrow peak in the invariant mass distribution of the e^+e^- pair from the subsequent decay $A' \to e^+e^-$. For the model with a dark photon, the obtained NA-48/2 constraints exclude the explanation of the $(g_\mu - 2)$ anomaly for the mass range $9 < m_{A'} < 70$ MeV [114] (see Fig. 15). We emphasize that the $\pi^0 \to \gamma A'$ decay width is proportional to $(g_{Vu}q_u - g_{Vd}q_d)^2 = (2g_{Vu} + g_{Vd})^2/9$ and for models with nonuniversal coupling constants of the A′ boson, for example, for a model with the L_μ–L_τ coupling, the NA-48/2-constraint [114] is not applicable.[26]

4.1.4 ATLAS and CMS constraints on light particles in Higgs boson decays. The ATLAS collaboration searched for a new γ_d particle in the Higgs boson decays $h \to 2\gamma_d + X$ and $h \to 4\gamma_d + X$ [116]. Under the assumption that the new γ_d boson decays mainly into a muon pair, constraints on the branching ratios (BRs) $BR(h \to 2\gamma_d + X)$ and $BR(h \to 4\gamma_d + X)$ were obtained [116]. We emphasize that, for the model with a dark photon, the constraint on the ϵ parameter is rather weak. The CMS collaboration also searched for new particles [117] in the Higgs boson decays $h \to 2a + X \to 4\mu + X$. Constraints similar to the corresponding ones in the ATLAS collaboration were obtained.

4.1.5 LHCb constraints on the decay $A' \to \mu^+\mu^-$. The LHCb collaboration searched for A′ bosons using the visible decay $A' \to \mu^+\mu^-$ [118]. The A′ were assumed to be produced either in direct pp collisions or in decays of $\pi^0(\eta)$ mesons [118]. Under the assumption that the A′ boson is produced due to nonzero $\gamma A'$ mixing, a constraint on the ϵ parameter was obtained in the A′ mass range from 214 MeV to 70 GeV for direct A′ decays and for $214 < m_{A'} < 350$ MeV for a long-lived A′ [118]. These constraints are currently the strongest in the mass range $10.6 < m_{A'} < 70$ GeV.

4.2 Invisible A′ decays

4.2.1 Constraints from the decay $K \to \pi$ + invisible. The light vector A′ boson can be produced in the decay $K \to \pi A'$, in full analogy with the well-known decay $K \to \pi\gamma^*$ of a K meson into a π meson and a virtual photon. For the model with the dominant decay of A′ into invisible modes, a nontrivial constraint on the mixing parameter of the A′ boson arises. Namely, the results of the BNL E949 and E787 experiments [119] measuring the $K^+ \to \pi^+\nu\bar{\nu}$ decay width were used to obtain the upper bound for $BR(K^+ \to \pi^+A')$ under the assumption that the $A' \to$ invisible decay dominates. In the model with a dark photon, the explanation for the $(g_\mu - 2)$ anomaly was excluded for $m_{A'} > 50$ MeV, except for a narrow region near $m_{A'} = m_\pi$ [120, 121]. We note that NA64 sets more stringent constraints on ϵ than E949 and E787 do (see Fig. 5).

[25] For $m_{A'} \gg m_e$, in view of chiral invariance, the constraints on g_{Ve} and g_{Ae} are identical.

[26] In [83], a model with $2g_{Vu} + g_{Vd} \approx 0$ was proposed as an explanation for a recent indication of the observation [82] of a narrow resonance with a mass of 17 MeV in a peak of the e^+e^- invariant mass distribution in nuclear transitions (see Section 3.3).

4.2.2 Electron–positron experiments. The BaBar collaboration [122] used the reaction $e^+e^- \to \gamma A'$, $A' \to$ invisible to search for invisible decays of the A' boson. Assuming that the invisible decays of A' dominate, we obtain the constraint $\epsilon \leqslant 10^{-3}$, which is independent of the mass of A' for $m_{A'} \leqslant 9.5$ GeV (see Fig. 5).

4.2.3 Electron beam-dump experiments. In electron beam-dump experiments, the reaction $eZ \to eZA'$ is used to produce an A' boson in a passive target. After passing through the protection necessary to suppress the backgrounds, A' bosons can manifest themselves in visible decays $A' \to e^+e^-$, $\mu^+\mu^-$. If A' decays mainly in the invisible modes into LDM particles, $A' \to \chi\bar{\chi}$, elastic scattering $\chi e \to \chi e$, $\chi N \to \chi N$ allows detecting LDM particles in the far detector. The results of electron beam-dump experiments at SLAC [123] and Fermilab [124] were used to obtain constraints on the A' coupling constants [125]. In the case of dominant decays of A' into invisible particles, these experiments exclude the range $10^{-7} \leqslant \epsilon \leqslant 10^{-6}$ for $m_{A'} \leqslant 20$ MeV (also see Fig. 6). At the same time, the E137 experiment yields the strongest constraints and excludes the parameter $y \equiv \epsilon^2 \alpha_D (m_\chi/m_{A'})^4$ at the level $y \geqslant 10^{-11}(10^{-9})$ for $m_{A'} \leqslant 1(100)$ MeV [125].

4.2.4 Proton beam-dump experiments. In proton experiments, the main source of A' bosons is the reaction $pZ \to \pi^0(\eta) + \ldots$ with the subsequent decays $\pi^0(\eta) \to \gamma A'$ of the π^0 and η mesons [126, 127]. In the case of a dominant A' decay into LDM particles, $A' \to \chi\bar{\chi}$, the scattering reactions $\chi e \to \chi e$ and $\chi N \to \chi N$ on electrons and nuclei are used to identify LDM in the target of the far detector.

The liquid scintillator neutrino detector (LSND) [128] at Los Alamos was designed primarily for neutrino detection. Neutrinos arise mainly from the reaction $pZ \to \pi^+ + \ldots$ with the subsequent decay $\pi^+ \to \mu^+\nu_\mu$. LSND data for $N = 10^{24}$ POT also allow restricting the coupling constants of a dark photon to quarks using the chain of processes $pZ \to \pi^0(\pi^0 \to \gamma A') + \ldots$ as the source of the A' boson. The resulting LSND constraints on the parameter $y \equiv \epsilon^2 \alpha_D (m_\chi/m_{A'})^4$ are usually much stronger than the corresponding constraints in the E137 experiment (see Fig. 6).

The MiniBooNE (BooNE: Booster Neutrino Experiment) experiment at Fermilab is also a proton beam-dump experiment using an 8-GeV booster. As in the LSND, dark photons are produced mainly in the decays of π^0 mesons and are detected in an 800-ton Cherenkov target detector located approximately 500 m away from the beam absorber. MiniBooNE obtained the parameter constraint $y \leqslant 10^{-8}$ for $\alpha_D = 0.5$ with DM particle masses $0.01 < m_\chi < 0.3$ GeV in a run with 1.86×10^{20} POT [129].

The main goal of the Coherent experiment [130] at Oak Ridge National Laboratory (USA) was to measure coherent elastic neutrino–nucleus scattering (CEvNS) and verify the quadratic dependence of the cross section on the number of nucleons in the nucleus. The results of measurements of the CEvNS cross section in the Coherent experiment [131] are in agreement with the SM predictions. Coherent is a beam-dump experiment, and LDM is formed mainly in the decays $\pi^0 \to \gamma A' \to \gamma\chi\bar{\chi}$ and can be identified by means of coherent elastic scattering with nucleus recoil. In [132], recent data from the Coherent experiment [131] were used to derive constraints on the LDM parameters. For $1 < m_\chi < 90$ MeV, a constraint on $\epsilon e_D^{1/2}$ was obtained, placing it between 10^{-5} and 10^{-4}.

4.3 Constraint from the $\nu_\mu N \to \nu_\mu N \mu^+\mu^-$ reaction

Studying muon pair production under the action of neutrinos in the Coulomb field of a nucleus, $\nu_\mu N \to \nu_\mu N \mu^+\mu^-$, allows constraining the model in which the Z' boson is coupled to the $L_\mu - L_\tau$ current. The data from the CHARM and CCFR (Chicago–Columbia–Fermilab–Rochester) experiments exclude a Z'-explanation of the $(g_\mu - 2)$ anomaly for the mass range $m_{Z'} \geqslant 400$ MeV [133].

4.4 Nonaccelerator constraints

In this section, for the sake of completeness, we briefly present the main astrophysical and cosmological constraints on the parameters of LDM models.

4.4.1 Constraints from cosmic microwave background radiation. Residual annihilation of DM particles after the stage of nonequilibrium annihilation but before the recombination stage can additionally ionize hydrogen atoms, thus modifying the CMB spectrum. The constraints obtained from the data of the Planck experiment [71] exclude s-wave annihilation of DM particles with a mass less than 10 GeV. The p-wave annihilation is allowed, because the cross section is suppressed by the factor T/m_χ. LDM models with pseudo-Dirac fermions [6, 54] are also possible.

4.4.2 Constraints coming from stars. Light A' bosons can be produced in stars. The possible loss of energy in stars, for example, in the Sun, due to the radiation of A' bosons allows obtaining strong constraints on the parameter $\epsilon \leqslant O(10^{-14})$ for masses $m_{A'} \leqslant 0.01$ MeV [134, 135]. In addition, for masses $m_{A'} \leqslant 0.3$ MeV, similar, but weaker, constraints on ϵ can be obtained from data on red giants [134, 135].

4.4.3 Constraints from the supernova SN1987a. The constraints from SN1987a are based on the fact that, if A' or other light particles are produced in large quantities, then they reduce the amount of emitted invisible energy in the form of neutrinos, which would contradict the experimental data. In [136], constraints on the ϵ parameter were obtained for the model with a dark photon. Constraints exist for masses $m_{A'} \leqslant 120$ MeV [136], and in the most interesting case $m_{A'} \geqslant 2m_e$, the resulting constraint $\epsilon \geqslant O(10^{-7})$ does not restrict LDM models too strongly.

4.4.4 Constraints from nucleosynthesis. Nucleosynthesis in the early Universe can be used to obtain constraints on the coupling constants of LDM models. During the first few minutes after the Big Bang, the temperature in the Universe dropped sharply due to the expansion of the Universe. During the expansion, some light elements were formed, and the prediction for the abundance of these elements in the Universe coincides with experimental data [137]. The constraints on new interactions are based on the fact that the existence of a new relativistic particle increases the rate of the expansion of the Universe. A higher expansion rate increases the temperature of the neutrino decoupling from equilibrium, and therefore the n/p ratio and hence the abundance of ^{4}He increase. The observed value of the density of ^{4}He allows constraining the coupling constants of a new hypothetical relativistic particle. For the model with a dark photon, constraints on the coupling constants were obtained in [138]. A dark photon with a mass $m_{A'} \leqslant (7\text{–}10)$ MeV is ruled out as a mediator between observable matter and DM [139]. We also note that the constraint $m_\chi \geqslant O(1)$ MeV on the masses of

LDM particles was obtained from the experimental constraint on the number of neutrinos [140].

4.5 Direct detection of light dark matter

The main problem arising in the detection of LDM particles via their scattering on nuclei is the small value of the nucleus recoil momentum [6]. The speed of DM particles $v_\chi \sim 10^{-3}c$, and the maximum possible energy transfer is proportional to the square of the effective mass $\mu_{\rm red} = m_{\rm nuclei} m_\chi/(m_{\rm nuclei} + m_\chi)$. The recoil energy of the nucleus is given by [6]

$$E_{\rm NR} = \frac{q^2}{2m_{\rm nuclei}} \leqslant \frac{2\mu_{\rm red}^2 v_\chi^2}{m_{\rm nuclei}} \leqslant 190 \text{ eV} \times \left(\frac{m_\chi}{500 \text{ MeV}}\right)^2 \left(\frac{16 \text{ GeV}}{m_{\rm nuclei}}\right), \qquad (59)$$

which makes the detection of LDM particles with a mass $m_\chi \leqslant O(1)$ GeV on nuclei an extremely difficult problem. There remains a possibility related to the use of elastic scattering on electrons [6]. For elastic scattering of LDM particles on an electron, the maximum possible energy transferred to the electron is

$$E_{\rm e} \leqslant \frac{1}{2} m_\chi v_\chi^2 \leqslant 3 \text{ eV} \left(\frac{m_\chi}{\text{MeV}}\right). \qquad (60)$$

Bound electrons with a binding energy $\Delta E_{\rm b}$ can generate a measurable signal if [6]

$$m_\chi \geqslant 0.3 \text{ MeV} \, \frac{\Delta E_{\rm b}}{1 \text{ eV}}. \qquad (61)$$

The nonrelativistic elastic cross section of scalar and Dirac LDM particles with $m_\chi \geqslant m_{\rm e}$ can be expressed as [6, 141]

$$\sigma(\text{e}\chi \to \text{e}\chi) = \frac{16\pi m_{\rm e}^2 \alpha \epsilon^2 \alpha_{\rm D}}{m_{\rm A'}^4}, \qquad (62)$$

whereas the elastic scattering of Majorana particles is suppressed by the factor $k_{\rm M} = (2m_{\rm e}^2/m_\chi^2) v_\chi^2$,

$$\sigma(\text{e}\chi_{\rm Majorana} \to \text{e}\chi_{\rm Majorana}) = \frac{16\pi m_{\rm e}^2 \alpha \epsilon^2 \alpha_{\rm D}}{m_{\rm A'}^4} k_{\rm M}, \qquad (63)$$

which makes the direct detection of Majorana particles in the model with a dark photon extremely difficult.

The XENON1T collaboration recently published new record-breaking results [142] on the search for elastic scattering of LDM particles by electrons. New constraints on the elastic scattering by electrons were obtained for $m_\chi \geqslant 30$ MeV. For the model with a dark photon, the use of formula (62) and the results in [142] allow obtaining a constraint on $\epsilon^2\alpha_{\rm D}$. In Fig. 16, we compare the upper bounds obtained at a 90% CL for the elastic cross section for electron scattering by LDM particles in the model with a dark photon based on the NA64 experiment [40] and the constraints obtained in the BaBar and XENON1T experiments [142] at $\alpha_{\rm D} = 0.1$. For $m_\chi \leqslant 50$ MeV, the NA64 constraint based on formula (63) for the elastic cross section of the scattering of LDM particles by an electron is stronger than the constraint from the XENON1T experiment. For pseudo-Dirac fermions with a moderate $\delta = (m_{\chi_2} - m_{\chi_1})/m_{\chi_1}$, the electroproduction reaction $\chi_1 \text{e} \to \chi_2 \text{e}$ for nonrelativistic χ_1 LDM particles is prohibited by virtue of the energy conservation law. Elastic scattering $\chi_1 \text{e} \to \chi_1 \text{e}$ is absent at the tree level, which makes LDM detection extremely difficult.

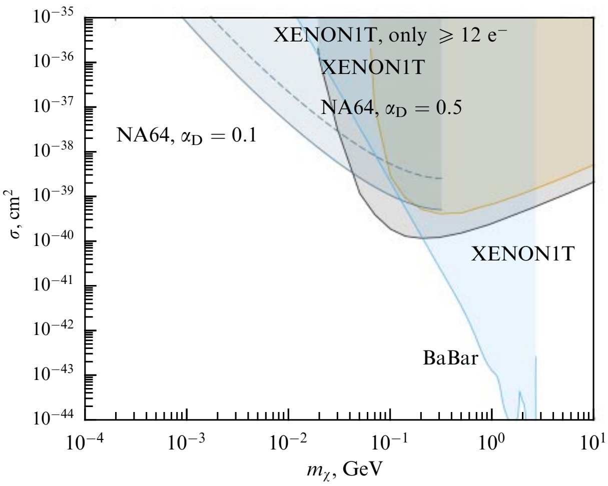

Figure 16. (Color online.) Comparison of upper bounds of the cross section of elastic scattering of LDM particles by an electron at a 90% CL obtained from NA64 [40] and BaBar constraints on the mixing parameter ϵ and from direct searches in the XENON1T experiment [142]. Blue curves are calculated for $\alpha_{\rm D} = 0.1$, dashed curve corresponds to $\alpha_{\rm D} = 0.5$, yellow curve shows XENON1T bounds obtained without considering signals with < 12 produced electrons (see [142]).

5. Other future experiments

At present, quite a few experiments are planned to search for A$'$ bosons and LDM using accelerators. In Sections 5.1–5.8, we briefly mention the most interesting experiments, from our point of view, on the search for A$'$ bosons for both the visible and invisible decay modes. A more detailed description can be found in review [143].

5.1 SHiP experiment at CERN

The SHiP (Search for Hidden Particles) experiment [144] at CERN involves the search for visible decays $\text{A}' \to \text{e}^+\text{e}^-$, $\mu^+\mu^-$, $\pi^+\pi^-$ of long-lived A$'$ bosons based on the use of an SPS beam. SHiP can also search for LDM by detecting elastic scattering of LDM particles by electrons and protons. It is expected that the main backgrounds associated with elastic neutrino scattering processes can be suppressed. For 2×10^{20} POT, the achievable sensitivity for $y \equiv \epsilon^2 \alpha_{\rm D} (m_\chi/m_{\rm A'})^4$ is $y \gtrsim 10^{-13}$ for $m_\chi \leqslant O(1)$ GeV [145, 146]. The experiment is under development.

5.2 Belle-II at KEK

Belle-II of the Japanese high-energy physics organization KEK [147, 148] is a multipurpose detector sensitive to invisible A$'$ decays by searching for monophotons in the reaction $\text{e}^+\text{e}^- \to \gamma$ ($\text{A}' \to \text{invisible}$) in the mass range $m_{\rm A'} \leqslant 9.5$ GeV. The Belle-II detector can also search for visible decays of the A$'$ boson. The first data with total luminosity $L_{\rm t} = 50$ ab^{-1} are planned to be obtained by 2025. The sensitivity to the ϵ parameter is expected to be up to $\epsilon^2 \geqslant 10^{-9}$ for $m_{\rm A'} < 9.5$ GeV.

5.3 MAGIX experiment at MESA

Visible dark photon decays are to be searched for using the MAGIX dipole spectrometer (MESA Gas Internal target eXperiment) (Mainz) using a polarized electron beam with the energy ~ 105 MeV. An electron beam with such parameters is expected to be obtained at the MESA (Mainz

Energy-recovering Superconducting Accelerator) [149]. The electroproduction reaction $eZ \to eZA'$ together with the visible decay mode $A' \to e^+e^-$ will be used to identify the A′ boson. The expected sensitivity to ϵ^2 for masses $10 < m_{A'} < 60$ MeV is $\simeq 10^{-9}$. It is also planned to search for invisible A′ decays into LDM particles [149]. The sensitivity to y is expected to reach $y = 10^{-14}$. The experiment has been approved. The first data collection is planned to start in 2023.

5.4 FASER experiment

In the FASER experiment (ForwArd Search ExpeRiment) [150] at CERN, proton collisions in the ATLAS experiment are used to search for dark photons and other new particles produced in the diffraction region of pp collisions. A′ bosons are produced mainly at small angles to the proton collision axis. Calculations show that the main production reactions A′ in proton-proton collisions are direct production $pp \to A'X$ as well as the production of A′ in $\pi^0(\eta) \to A'\gamma$ decays. It is assumed that long-lived A′ bosons decay into e^+e^- and $\mu^+\mu^-$ pairs at an installation located at a distance of 480 m from the collision point. The signature of such a decay is the presence of two high-energy tracks of charged particles with a small angle between them and a common vertex. Calculations show that, for the integrated luminosity of the ATLAS experiment $L = 300$ fb^{-1}, FASER is sensitive to A′ decays with masses 10 MeV $\leqslant m_{A'} \leqslant$ 1 GeV and the mixing parameter $10^{-6} \leqslant \epsilon \leqslant 10^{-3}$.

5.5 PADME experiment

In PADME (Positron Annihilation into Dark Matter Experiment) in Frascati (Italy), the scattering reaction of positrons with the energy $\lesssim$500 MeV by electrons of a thin target, $e^+e^- \to \gamma A'$, including resonant A′ production, is used to search for a dark photon decaying in both visible and invisible modes [151, 152]. At 10^{13} POT, a sensitivity to the ϵ^2 parameter of up to 10^{-7} is expected for $m_{A'} < 24$ MeV [151, 152]. The experiment has been approved.

5.6 BDX experiment at the Jefferson Laboratory

BDX is a Beam-Dump eXperiment involving an intense beam of 10.6-GeV electrons at the Jefferson Laboratory (JLab) (USA) [153, 154]. The LDM particles produced in the target in the process $eZ \to eZA'$; $A' \to \chi\bar{\chi}$ pass through a protecting shield and are detected via elastic scattering $e\chi \to e\chi$ on electrons in the far detector. The expected sensitivity to the y parameter is at the level $y \geqslant 10^{-13}$ for $1 < m_\chi < 100$ MeV. The experiment has been approved.

5.7 DarkLight experiment at the Jefferson Laboratory

In the DarkLight experiment, dark photons are produced in the reaction $ep \to epA'$ in collisions of 100-MeV electrons in a gaseous hydrogen target [154, 155]. The main feature of the experiment is the possibility of detecting a scattered electron and a recoil proton, and hence the ability to reconstruct invisible decays of A′. It is also possible to search for visible $A' \to e^+e^-$ decays. A sensitivity at the level $\epsilon^2 \geqslant 10^{-6}$ is expected for masses $10 < m_{A'} < 80$ MeV. The experiment has been approved.

5.8 LDMX

LDMX (Light Dark Matter eXperiment) is an experiment similar to NA64, with the A′ electroproduction reaction on a thin target, $eZ \to eZA'$, $A' \to \chi\bar{\chi}$, to be used to search for the

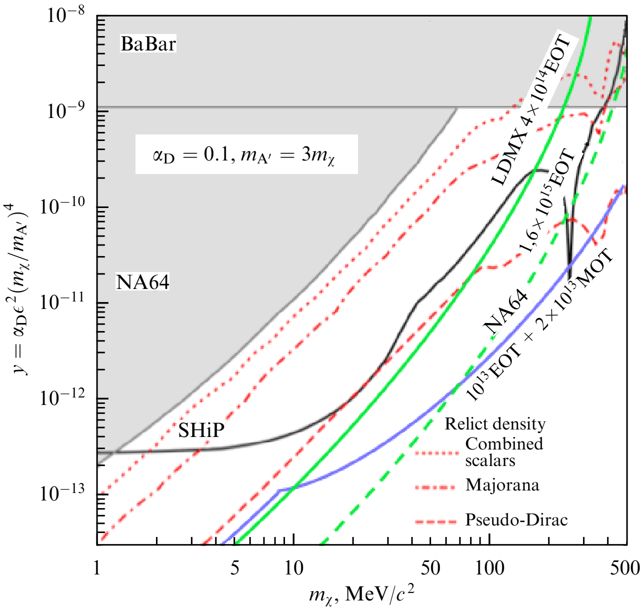

Figure 17. (Color online.) Comparison at a 90% CL of search prospects for LDM in NA64, LDMX, and SHiP experiments. Black solid line shows the sensitivity of the SHiP experiment. Green solid (dashed) curve corresponds to the LDMX experiment with incident electron energy $E_e = 4$ GeV and $N_{EOT} = 4 \times 10^{14}$ ($E_e = 8$ GeV and $N_{EOT} = 1.6 \times 10^{15}$). Blue curve corresponds to expectations of the NA64 experiment from combined data with $N_{EOT} = 10^{13}$ and $N_{MOT} = 2 \times 10^{13}$ under the assumption of a negligibly low background level.

dark photon at incident electron energies of 4 and 8 GeV [156]. Unlike NA64, LDMX is capable of measuring both the missing energy and the missing momentum, which can be important for better suppression of the backgrounds. A sensitivity to the ϵ parameter of up to 10^{-6} is expected at $m_{A'} = 1$ MeV [156]. The modified LDMX will be able to improve the sensitivity to the ϵ parameter by an order of magnitude, to 10^{-7} [156].

Figure 17 shows prospects for the LDM search based on the use of the invisible decay mode of the dark photon into LDM particles for the three most interesting experiments: NA64, LDMX, and SHiP. It can be seen from the figure that the prospects for NA64 and the first stage of LDMX with energies of electrons incident on the target $E_e = 4$ GeV and with $N_{EOT} = 4 \times 10^{14}$ are comparable. When the second phase of LDMX with the energy $E_e = 8$ GeV and $N_{EOT} = 1.6 \times 10^{15}$ is realized, LDMX will have a better sensitivity to the search for LDM. The experiment is currently at the development stage.

6. Conclusion

LDM models that are renormalizable extensions of the SM explain the origin of DM and its observed relict density in the Universe by introducing a new interaction between the hidden and visible sectors, realized by a light mediator. It is surprising that predictions of the masses and coupling constants of LDM particles and the mediators of new interactions lie in a range accessible to searches in modern accelerators, which makes them extremely attractive for experimenters, stimulating additional efforts to develop new methods and improve the sensitivity of LDM search experiments.

One such approach, developed in the NA64 experiment, is based on the search for energy nonconservation in the processes of scattering of charged leptons by a nucleus. These processes are also of great interest because their observation would clearly go beyond the framework of the SM and require its significant extension. The very fact of the discovery of DM in the Universe without a doubt increases interest in such searches and gives hope for obtaining experimental indications of the existence of LDM in the near future. Negative results would allow excluding this class of models, thereby narrowing the range of viable candidates.

The search for LDM in missing-energy events based on the active beam-dump method in the NA64 experiment has allowed obtaining record constraints on the parameters of LDM models with a vector mediator. Future NA64 searches using electron and muon beams and especially their combined results have good prospects in a wide range of parameters of LDM models in the mass range 1 MeV $\leqslant m_{\mathrm{A}'} \leqslant$ 1 GeV. With the statistic of 5×10^{12} EOT, the NA64 is able to test scalar and Majorana LDM models with the mass ratio $m_{\mathrm{A}'}/m_\chi \geqslant 2.5$. The joint results of NA64e and NA64μ obtained with electron and muon beams for $\gtrsim 10^{13}$ EOT and 2×10^{13} MOT will allow exploring the region of model parameters with a pseudo-Dirac LDM for $m_{\mathrm{A}'}/m_\chi \geqslant 3$. This makes NA64e and NA64μ complementary and significantly increases the chances of discovering LDM.

There are several alternatives to the model with a dark photon based on the use of gauge symmetries such as $L_\mu - L_\tau$, $\mathrm{U}(1)_{B-L}$, or $\mathrm{U}(1)_{B-3\mathrm{e}}$ [6, 11]. As in the model with a dark photon, the observed value of the DM energy density allows estimating the parameter ϵ of the coupling of a new light Z' boson to the electron. The ϵ value in such models is the same as in the model with a dark photon up to a factor $k \leqslant 3$ [6, 11], and therefore NA64e can test these models as well. For example, for a model with the vector $B-L$ coupling, NA64e is able to exclude scalar and Majorana LDM models, in full analogy with the model with a dark photon. However, we emphasize that, because the annihilation cross section is proportional to $(m^2_{\mathrm{A}'} - 4m^2_\chi)^{-2}$ in the resonance region with $m_{\mathrm{A}'} \approx 2m_\chi$ and the predicted value of ϵ^2 is inversely proportional to the cross section, this can reduce the value of ϵ^2 by 2 to 4 orders of magnitude compared with that in the case of the frequently considered reference point $m_{\mathrm{A}'}/m_\chi = 3$ [6]. This means that the study of the range of parameters $m_{\mathrm{A}'} \approx 2m_\chi$ would require additional effort from both NA64 and planned experiments [144–156].

The established accelerator experimental constraints significantly narrow the possibilities of explaining the muon $(g_\mu - 2)$ anomaly by the existence of a new light boson, although not completely eliminating this hypothesis.[27] The most popular model, in which the dark photon A' interacts with the electromagnetic current due to a nonzero mixing, is ruled out by NA64 [38] and BaBar [122]. The coupling of the Z' boson to the $L_\mu - L_\tau$ current, which explains the muon $(g_\mu - 2)$ anomaly, is excluded for $m_{\mathrm{Z}'} \geqslant 2m_\mu$. The search for Z' with a mass in the range $m_{\mathrm{Z}'} \leqslant 2m_\mu$ is planned in the NA64μ experiment.

The nature and origin of DM have not yet been established. In the near future, important experiments on the DM search will be carried out. These experiments, such as NA64, Belle-II, LDMX, and others, will be very challenging. But they have good prospects of detecting LDM, if it exists, after several years of operation.

[27] A review of nonaccelerator constraints is available in [157].

Acknowledgments. We are grateful to our colleagues from the NA64 collaboration and, in particular, S V Donskov, D V Kirpichnikov, M M Kirsanov, P Crivelli, V E Lyubovitsky, V A Polyakov, and V D Samoylenko for their many helpful discussions and comments. We are also grateful to colleagues from the Theoretical Department of the Institute for Nuclear Research, Russian Academy of Sciences, and the Bogoliubov Laboratory of Theoretical Physics of the Joint Institute for Nuclear Research for their interest in this work and comments. We are grateful to R Dusaev for his help in preparing some figures and to Yu M Andreev for the careful reading of the manuscript and helpful comments.

This study was carried out with the financial support of the Russian Foundation for Basic Research in the framework of research project 20-12-50027.

References

1. Kolb E W, Turner M *The Early Universe* (Frontiers in Physics, Vol. 69) (Reading, Mass.: Addison-Wesley, 1990)
2. Gorbunov D S, Rubakov V A *Introduction to the Theory of the Early Universe. Cosmological Perturbations and Inflationary Theory* (Singapore: World Scientific, 2011) https://doi.org/10.1142/7873
3. Clifton T et al. *Phys. Rep.* **513** 1 (2012)
4. Boehm C, Fayet P *Nucl. Phys. B* **683** 219 (2004)
5. Essig R et al., Report of the Community Summer Study 2013 (Snowmass) Intensity Frontier New, Light, Weakly-Coupled Particles subgroup; arXiv:1311.0029
6. Alexander J et al., Dark Sectors 2016 Workshop: Community Report; arXiv:1608.08632
7. Battaglieri M et al., U.S. Cosmic Visions: New Ideas in Dark Matter (2017); arXiv:1707.04591
8. Beacham J et al. *J. Phys. G* **47** 010501 (2020)
9. Fabbrichesi M, Gabrielli E, Lanfranchi G *The Physics of the Dark Photon. A Primer* (SpringerBriefs in Physics) (Cham: Springer, 2021) https://doi.org/10.1007/978-3-030-62519-1; arXiv:2005.01515
10. Lee H-S *Phys. Rev. D* **90** 091702 (2014)
11. Berlin A et al. *Phys. Rev. D* **99** 075001 (2019)
12. Agrawal P et al., arXiv:2102.12143
13. Lee B W, Weinberg S *Phys. Rev. Lett.* **39** 165 (1977)
14. Vysotskii M I, Dolgov A D, Zel'dovich Ya B *JETP Lett.* **26** 188 (1977); *Pis'ma Zh. Eksp. Teor. Fiz.* **26** 200 (1977)
15. Zyla P A et al. (Particle Data Group) *Prog. Theor. Exp. Phys.* **2020** 083C01 (2020)
16. Izaguirre E et al. *Phys. Rev. D* **91** 094026 (2015)
17. Krnjaic G *Phys. Rev. D* **94** 073009 (2016)
18. Chen C-Y, Pospelov M, Zhong Y-M *Phys. Rev. D* **95** 115005 (2017)
19. Okun' L B *Sov. Phys. JETP* **56** 502 (1982); *Zh. Eksp. Teor. Fiz.* **83** 892 (1982)
20. Holdom B *Phys. Lett. B* **166** 196 (1986)
21. He X-G et al. *Phys. Rev. D* **43** 22 (1991)
22. Foot R *Mod. Phys. Lett. A* **76** 527 (1991)
23. He X-G et al. *Phys. Rev. D* **44** 2118 (1991)
24. Krasnikov N V, arXiv:1707.00508
25. Gninenko S N, Krasnikov N V *Phys. Lett. B* **783** 24 (2018)
26. Chen C-Y, Kozaczuk J, Zhong Y-M *J. High Energy Phys.* **2018** (10) 154 (2018)
27. Escudero M et al. *J. High Energy Phys.* **2019** (03) 071 (2019)
28. Abi B et al. (Muon g-2 Collab.) *Phys. Rev. Lett.* **126** 141801 (2021)
29. Davier M et al. *Eur. Phys. J. C* **71** 1515 (2011)
30. Jegerlehner F, Szafron R *Eur. Phys. J. C* **71** 1632 (2011)
31. Hagiwara K et al. *J. Phys. G* **38** 085003 (2011)
32. Aoyama T et al. *Phys. Rev. Lett.* **109** 111808 (2012)
33. Gninenko S N, Krasnikov N V *Phys. Lett. B* **513** 119 (2001)
34. Baek S et al. *Phys. Rev. D* **64** 055006 (2001)
35. Ma E, Roy D P, Roy S *Phys. Lett. B* **525** 101 (2002)
36. Krasnikov N V, arXiv:1702.04596
37. Andreas S et al., arXiv:1312.3309

38. Banerjee D et al. (NA64 Collab.) *Phys. Rev. Lett.* **118** 011802 (2017)
39. Banerjee D et al. (NA64 Collab.) *Phys. Rev. D* **97** 072002 (2018)
40. Banerjee D et al. (NA64 Collab.) *Phys. Rev. Lett.* **123** 121801 (2019)
41. Banerjee D et al. (NA64 Collab.) *Phys. Rev. Lett.* **120** 231802 (2018)
42. Banerjee D et al. (NA64 Collab.) *Phys. Rev. Lett.* **125** 081801 (2020)
43. Andreev Yu M et al. (NA64 Collab.) *Phys. Rev. Lett.* **126** 211802 (2021)
44. Gross G, Lebedev O, Mambrini Y *J. High Energy Phys.* **2015** (08) 158 (2015)
45. Chen C-R, Chu Y-K, Tsai H-C *Phys. Lett. B* **741** 205 (2015)
46. Berlin A et al. *Phys. Rev. D* **97** 055033 (2018)
47. Ramos R, Tran V Q, Yuan T-C *J. High Energy Phys.* **2021** 112 (2021); arXiv:2109.03185
48. Dolgov A D et al. *Phys. Rev. D* **88** 117701 (2013)
49. Liu et al. *Phys. Rev. D* **100** 123011 (2019)
50. Gninenko S N, Kirpichnikov D V, Krasnikov N V *Phys. Rev. D* **100** 035003 (2019)
51. Mondino C et al. *Phys. Rev. D* **103** 035027 (2021)
52. Darmé L, Rao S, Roszkowski L *J. High Energy Phys.* **2018** (12) 014 (2018)
53. Darmé L, Rao S, Roszkowski L *J. High Energy Phys.* **2018** (03) 084 (2018)
54. Smith D, Weiner N *Phys. Rev. D* **64** 043502 (2001)
55. Davoudiasl H, Marciano W J *Phys. Rev. D* **92** 035008 (2015)
56. Gherghetta T et al. *Phys. Rev. D* **100** 095001 (2019)
57. Gninenko S N, Krasnikov N V, Matveev V A *Phys. Part. Nucl.* **51** 829 (2020); *Fiz. Elem. Chast. Atom. Yad.* **51** 983 (2020)
58. Cazzaniga C et al. (NA64 Collab.) *Eur. Phys. J. C* **81** 959 (2021); arXiv:2107.02021
59. Bjorken J D et al. *Phys. Rev. D* **80** 075018 (2009)
60. Liu Y-S , Miller G A *Phys. Rev. D* **96** 016004 (2017)
61. Gninenko S N et al. *Phys. Lett. B* **782** 406 (2018)
62. Gninenko S N *Phys. Rev. D* **89** 075008 (2014)
63. Bevan A J et al. *Eur. Phys. J. C* **74** 3026 (2014)
64. Bennett G W et al. (Muon g-2 Collab.) *Phys. Rev. D* **73** 072003 (2006)
65. Dorokhov A E, Radzhabov A E, Zhevlakov A S *EPJ Web Conf.* **125** 02007 (2016)
66. Jegerlehener F, Nyffeler A *Phys. Rep.* **477** 1 (2009)
67. Gninenko S N, Krasnikov N V *EPJ Web Conf.* **125** 02001 (2016)
68. Gondolo P, Gelmini G *Nucl. Phys. B* **360** 145 (1991)
69. Sherrer R J, Turner M S *Phys. Rev. D* **33** 1585 (1986)
70. Cline J M et al. *Phys. Rev. D* **88** 055025 (2013)
71. Ade P A R et al. *Astron. Astrophys.* **594** A13 (2016)
72. Holst I, Hooper D, Krnjaic G, arXiv:2107.09067
73. Gninenko S N et al. *Phys. Rev. D* **94** 095025 (2016)
74. Banerjee D, Crivelli P, Rubbia A *Adv. High Energy Phys.* **2015** 105730 (2015)
75. Volkov V Yu et al. *Phys. Part. Nucl. Lett.* **16** 847 (2019); *Pis'ma Fiz. Elem. Chast. Atom. Yad.* **16** 627 (2019)
76. Depero E et al. *Nucl. Instrum. Meth. Phys. Res. A* **866** 196 (2017)
77. Agostinelli S et al. *Nucl. Instrum. Meth. Phys. Res. A* **506** 250 (2003)
78. Bondi M et al. *Comput. Phys. Commun.* **269** 108129 (2021); arXiv:2101.12192
79. Antcheva I et al. *Comput. Phys. Commun.* **182** 1384 (2011)
80. Gninenko S N et al. *Phys. Lett. B* **796** 117 (2019)
81. Feng J L, Smolinsky J *Phys. Rev. D* **96** 095022 (2017)
82. Krasznahorskay A J et al. *Phys. Rev. Lett.* **116** 042501 (2016)
83. Feng J L et al. *Phys. Rev. D* **95** 035017 (2017)
84. Kozaczuk J *Phys. Rev. D* **97** 015014 (2018)
85. Chiang C-W, Tseng P-Y *Phys. Lett. B* **767** 289 (2017)
86. Zhang X, Miller G A *Phys. Lett. B* **773** 159 (2017)
87. Alikhanov I E, Paschos E A *Phys. Rev. D* **97** 115004 (2018)
88. Liang Y, Chen L-B, Qiao C-F *Chinese Phys. C* **41** 063105 (2017)
89. Fornal B *Int. J. Mod. Phys. A* **32** 1730020 (2017)
90. Fayet P *Eur. Phys. J. C* **77** 53 (2017); arXiv:1611.05357
91. Depero E et al. (NA64 Collab.) *Eur. Phys. J. C* **80** 1159 (2020)
92. Krasznahorkay A J et al., arXiv:1910.10459
93. Weinberg S *Phys. Rev. Lett.* **40** 223 (1978)
94. Wilczek F *Phys. Rev. Lett.* **40** 279 (1978)
95. Peccei R D, Quinn H R *Phys. Rev. Lett.* **38** 1440 (1977)
96. Kim J E *Phys. Rep.* **150** 1 (1987)
97. Raffelt G G *Phys. Rep.* **198** 1 (1990)
98. Parker R H et al. *Science* **360** 191 (2018)
99. Morel L et al. *Nature* **588** 61 (2020)
100. Aoyama T, Kinoshita T, Nio M *Atoms* **7** 28 (2019)
101. Hanneke D, Fogwell S, Gabrielse G *Phys. Rev. Lett.* **100** 120801 (2008)
102. Giudice G F, Paradisi P, Passera M *J. High Energy Phys.* **2012** (11) 113 (2012)
103. Davoudiasl H, Marciano W J *Phys. Rev. D* **98** 075011 (2018)
104. Endo M, Hamaguchi K, Mishima G *Phys. Rev. D* **86** 095029 (2012)
105. Krasnikov N V *Mod. Phys. Lett. A* **35** 2050116 (2020)
106. Gninenko S N, Krasnikov N V, Matveev V A *Phys. Rev. D* **91** 095015 (2015)
107. Banerjee D et al. (NA64 Collab.) "Proposal for an experiment to search for dark sector particles weakly coupled to muon at the CERN SPS", Preprint CERN-SPSC-2019-002 (2019)
108. Kirpichnikov D V et al. *Phys. Rev. D* **104** 076012 (2021); arXiv:2107.13297
109. Groom D E, Mokhov N V, Striganov S I *Atom. Data Nucl. Data Tabl.* **78** 183 (2001)
110. Abrahamyan S et al. *Phys. Rev. Lett.* **107** 191804 (2011)
111. Merkel H et al. (A1 Collab.) *Phys. Rev. Lett.* **112** 221802 (2014)
112. Lees J P et al. (BaBar Collab.) *Phys. Rev. Lett.* **113** 201801 (2014)
113. Pérez del Río E *Acta Phys. Pol. B* **47** 461 (2016)
114. Batley J R et al. (NA48/2 Collab.) *Phys. Lett. B* **746** 178 (2015)
115. Lees J P et al. (BaBar Collab.) *Phys. Rev. D* **94** 011102 (2016)
116. Aad G et al. (ATLAS Collab.) *J. High Energy Phys.* **2016** (02) 062 (2016)
117. Khachatryan V et al. (CMS Collab.) *Phys. Lett.* **752** 146 (2016)
118. Aaij R et al. (LHCb Collab.) *Phys. Rev. Lett.* **120** 061801 (2018)
119. Artamonov A V et al. (E949 Collab.) *Phys. Rev. D* **79** 092004 (2009)
120. Pospelov M *Phys. Rev. D* **80** 095002 (2009)
121. Essig R et al. *J. High Energy Phys.* **2013** (11) 167 (2013)
122. Lees J P et al. *Phys. Rev. Lett.* **67** 2942 (1991)
123. Bjorken J D et al. *Phys. Rev. D* **38** 3375 (1988)
124. Bross A et al. *Phys. Rev. Lett.* **67** 2942 (1991)
125. Batell B, Essig R, Surujon Z *Phys. Rev. Lett.* **113** 171802 (2014)
126. Gninenko S N *Phys. Rev. D* **85** 055027 (2012)
127. Gninenko S N *Phys. Lett. B* **713** 244 (2012)
128. Auerbach L B et al. (LSND Collab.) *Phys. Rev. D* **63** 112001 (2001)
129. Aguilar-Arevalo A A et al. (MiniBooNE-DM Collab.) *Phys. Rev. Lett.* **118** 221803 (2017)
130. Akimov D et al., arXiv:1803.09183
131. Akimov D et al. *Science* **357** 1123 (2017)
132. Ge S-F, Shoemaker I M *J. High Energy Phys.* **2018** (11) 066 (2018)
133. Almannsofer W et al. *Phys. Rev. Lett.* **113** 091801 (2014)
134. Redondo J, Raffelt G *JCAP* **2013** (08) 034 (2013)
135. An H, Pospelov M, Pradler J *Phys. Lett. B* **725** 190 (2013)
136. Chang J H, Essig R, McDermott S D *J. High Energy Phys.* **2018** (09) 051 (2018)
137. Wagoner R V, Fowler W A, Hoyle F *Astrophys. J.* **148** 3 (1967)
138. Fradette A et al. *Phys. Rev. D* **90** 035022 (2014)
139. Ahlgren B, Ohlsson T, Zhou S *Phys. Rev. Lett.* **111** 199001 (2013)
140. Boehm C, Dolan M J, McCabe C *JCAP* **2013** (08) 041 (2013)
141. Essig R, Mardon J, Volanski T *Phys. Rev. D* **85** 076007 (2012)
142. Aprile E et al. (XENON Collab.) *Phys. Rev. Lett.* **122** 141301 (2019)
143. Beacham J et al. *J. Phys. G* **47** 010501 (2020)
144. Alekhin S et al. *Rep. Prog. Phys.* **79** 124201 (2016)
145. Ahdida C et al. (SHiP Collab.) *J. High Energy Phys.* **2021** (04) 199 (2021)
146. Ahdida C et al. (SHiP Collab.) *Eur. Phys. J. C* **81** 451 (2021)
147. Kou E et al. *Prog. Theor. Exp. Phys.* **2019** 123C01 (2019); arXiv:1808.10567
148. Corona L *J. Phys. Conf. Ser.* **1526** 012031 (2020)
149. Doria L et al., arXiv:1809.07168
150. Feng J L et al. *Phys. Rev. D* **97** 035001 (2018)
151. Kozhuharov V *Nuovo Cimento C* **40** 5 192 (2017)
152. Spagnolo S (PADME Collab.) *J. Phys. Conf. Ser.* **1137** 012043 (2018)
153. Battaglieri M et al., arXiv:1712.01518
154. Celentano A *J. Phys. Conf. Ser.* **770** 012040 (2016)
155. Balewski J et al., arXiv:1412.4717
156. Åkesson T et al., arXiv:1808.05219
157. Jeong Y S, Kim C S, Lee H-S *Int. J. Mod. Phys. A* **31** 1650059 (2016)

158. Essig R et al. *J. High Energy Phys.* **2013** (11) 167 (2013)
159. Lees J P et al. (BaBar Collab.) *Phys. Rev. Lett.* **119** 131804 (2017)
160. Cortina E et al. (NA62 Collab.) *J. High Energy Phys.* **2019** (05) 182 (2019)
161. Demidov S, Gninenko S, Gorbunov D *J. High Energy Phys.* **2019** (07) 162 (2019)
162. Izaguirre E et al. *Phys. Rev. Lett.* **115** 251301 (2015)
163. Izaguirre E et al. *Phys. Rev. D* **96** 055007 (2017)
164. deNiverville P, Pospelov M, Ritz A *Phys. Rev. D* **84** 075020 (2011)
165. Batell B, Pospelov M, Ritz A *Phys. Rev. D* **80** 095024 (2009)
166. Batell B, Essig R, Surujon Z *Phys. Rev. Lett.* **113** 171802 (2014)
167. Aguilar-Arevalo A A et al. (The MiniBooNE-DM Collab.) *Phys. Rev. D* **98** 112004 (2018)
168. Essig R et al. *Phys. Rev. Lett.* **109** 021301 (2012)
169. Kahn Y et al. *J. High Energy Phys.* **2018** (09) 153 (2018)